CHAPTER IV

RESULTS AND DISCUSSION

This study was undertaken to fabricate a porous bone replacement with high mechanical strength and excellent biocompatibility by a combination of the use of additives (silica and glass frit). In this chapter, the experimental results and discussion are described in three main parts. In the first part, the property of as-received hydroxyapatite is discussed. In the second part, a study of the effect of additive content, silica, and glass frit on mechanical properties and bioactivity of porous hydroxyapatite using uniaxial pressing. This method for fabrication of HA samples was used to primary study. The final part concerns the fabrication and study of the effect of glass frit on mechanical properties of porous hydroxyapatite using polymeric sponge method. The mechanical properties and bioactivity of the samples were investigated in order to evaluate the possibility of using these samples as bone replacement.

4.1. Porous Hydroxyapatite using Uniaxial Pressing

4.1.1 Characterizations of as-received HA Powder

SEM micrographs and an X-ray diffraction pattern of as-received calcium phosphate powder are shown in Figure 4.1. The structure of calcium phosphate powder is composed of hydroxyapatite [$Ca_{10}(PO_4)_6(OH)_2$;HA] phase and all the peaks corresponded to the standard JCPDS card no. 09-0432 for HA phase. No additional phase could be identified. Secondary phases such as tricalcium phosphate (TCP), tetracalcium phosphate (TTCP) were not evident in the HA as-received powder. The average particle size of pure HA powder measured in the nanometer range consisted of

plates and irregular shapes. EDS results in Figure 4.2 confirmed that the main elements present in the HA powder are calcium, phosphorus and oxygen.

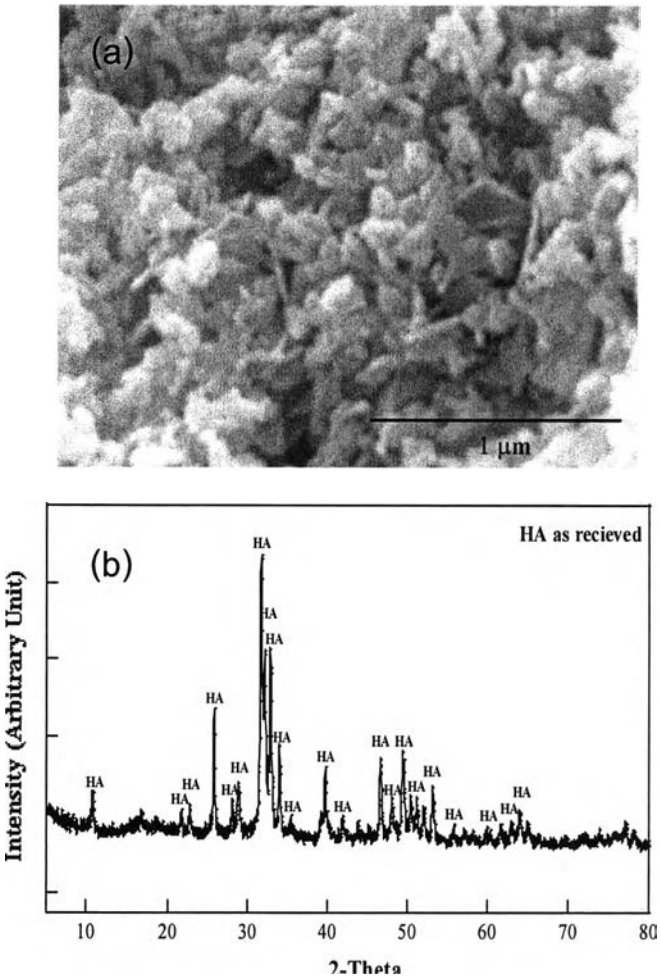

Figure 4.1 (a) SEM micrographs and (b) X-ray diffraction pattern of as-received HA powder.

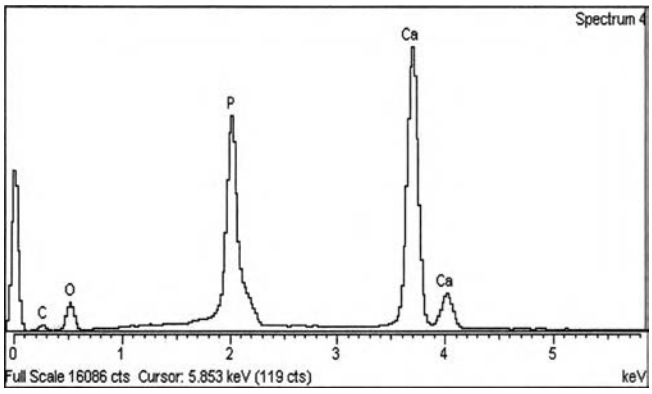

Figure 4.2 EDS analysis of as-received HA powder.

4.1.2 Microstructural Evolution of Pure HA After Sintering

The morphology and microstructure of sintered HA were examined using SEM. Figure 4.3 shows crystalline morphology of a pellet formed of HA powder fabricated by uniaxial pressing at 14 MPa and sintered at different temperatures. Grain size of HA rapidly increased with increasing sintering temperature. The measured grain sizes of HA were about 1.5 μm for sintering at 1150 °C and larger than 5 μm for 1300 °C. Additionally, SEM micrograph for HA sintered at 1300 °C showed clear distinction of grain boundaries and the grain diameter could be easily calculated, whereas in HA sintered at 1150 °C, the grain boundaries were less prominent. The bulk density variation of the HA samples sintered was found to increase with increasing sintering temperature. Sintered densities for pure HA at 1150 °C and 1300 °C were 2.3 and 3.0 g/cm^3, respectively. The increasing of density HA samples were similar to general ceramics that it increased with increasing sintering temperature [45].

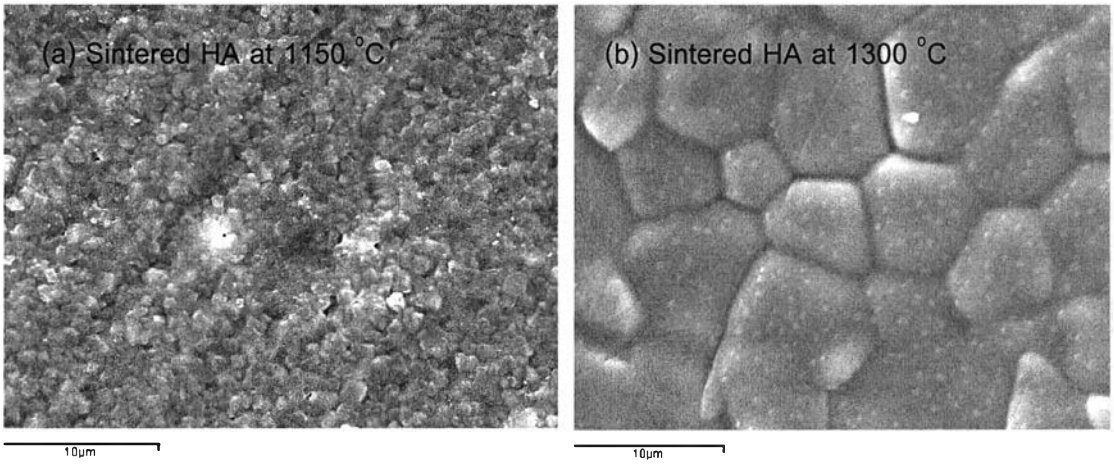

Figure 4.3 SEM micrographs of hydroxyapatite sintered at 1150 °C and 1300 °C, respectively.

4.1.3 Phase Formation of Pure HA After Sintering

The XRD analysis of the samples, regardless of sintering method indicated secondary phases were present in the HA lattice (Figure 4.4). After sintering, the crystallinity of sintered HA is much higher than that of the unsintered HA. The pure HA sintered at 1150°C shows diffraction peaks of HA and β-TCP phase, indicating some decomposition of HA to β-tricalcium phosphate (β-TCP; JCPDS Card No.09-0169). It is well known that pure hydroxyapatite is a thermally unstable compound, decomposing and transforming to TCP ($Ca_3(PO_4)_2$) at temperatures from about 800 to 1200 °C depending on its stoichiometry [27,38]. Therefore, HA sintered at 1150°C became a biphasic mixture of HA/β-TCP. Biphasic calcium phosphates (BCP), which are mixtures of HA and β-tricalcium phosphate are commonly used as bone substitutes. It is important to obtain an efficient bone substitute that can be degraded by bone cells and therefore be replaced by natural bone. It has been reported that the solubility and biodegradation rate of β-TCP are much higher than that of HA. Therefore, the combination of HA and β-TCP may lead to the formation of highly biodegradable biphasic calcium phosphates. Additionally, the crystallinity of the hydroxyapatite decreases with increasing temperature and may be become α-TCP at higher temperature. This result supported by FT-IR analysis of sintered HA with different sintering temperature is shown in Figure 4.5. These figure presents the FT-IR spectra patterns of HA as received and sintered at 1150 and 1300 °C. The characteristic bands at 1092, 1044, 1036, 960, 573 and 475 cm^{-1} were assigned to the vibration in the phosphate group of HA. In the spectra of HA powder, the broad band at about 3400 cm^{-1} corresponds to the absorbed hydrate and the sharp peak between 3570 and 630 cm^{-1} belongs to the stretching vibration of lattice OH ions [58,59]. The intensities at 3570 and 630 cm^{-1} (hydroxyl stretching bands) of HA drastically decrease with increasing sintering temperature compared with those of the hydroxyapatite spectra. The decreasing of the bands at 3570 and 630 cm^{-1} (derived from the hindered rotation made of OH^- group in HA) further confirm the phase transformation of HA to β-TCP and α-TCP.

The presence of a phase transformation is common for HA ceramics sintered at high temperature.

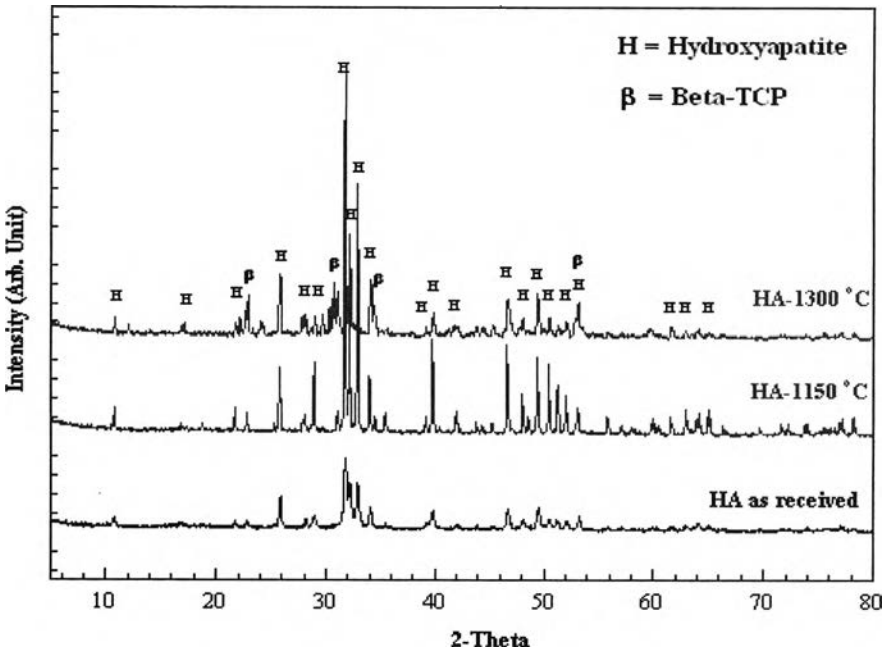

Figure 4.4 X-ray diffraction patterns of hydroxyapatite as received and sintered at 1150 °C and 1300 °C.

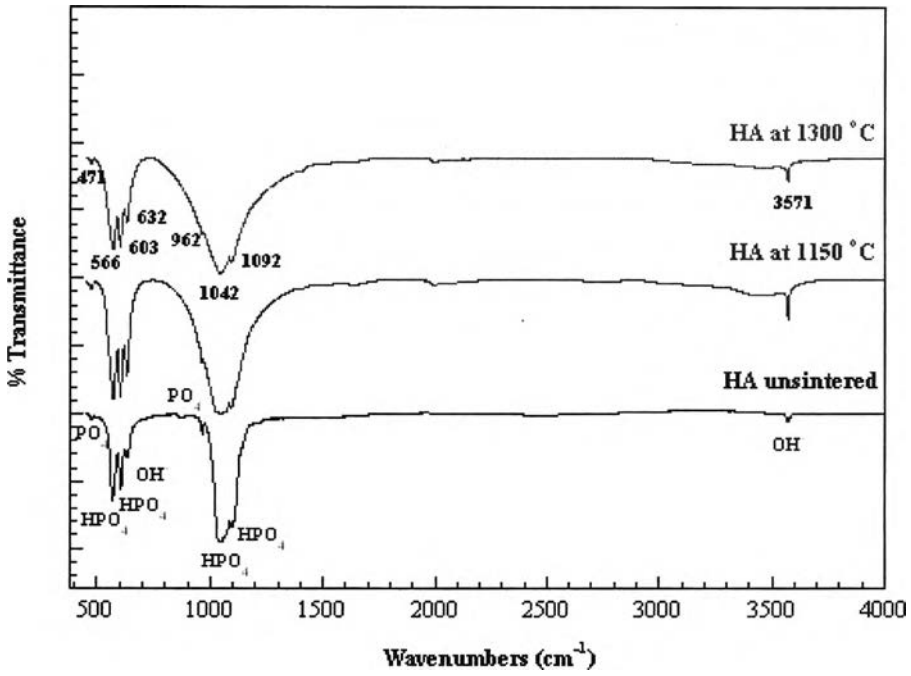

Figure 4.5 FT-IR spectra of hydroxyapatite as received and sintered at 1150 °C and 1300 °C.

4.1.4 *In vitro* Bioactivity of Pure HA

Biomaterials for bone substitutions require a degree of bioactivity, which is an ability to form a bonding layer with a bone-like apatite structure in order to accelerate bone growth. The *in-vitro* bioactivity can be predicted by examining Ca-P apatite formation on the surfaces of substrate materials immersed in SBF, which has an ion concentration similar to that of human blood plasma. Therefore, the aim of this topic was to study the formation of the Ca-P apatite layer on the surface of HA by immersing the samples in SBF for varied periods. The SEM micrographs of HA after immersion in SBF are shown in Figure 4.6, which display the precipitate nucleation and growth with immersion time on the sample surface. Before immersion, no degradation and precipitation were observed. After 6 h immersed in SBF, the cluster of mineral precipitated detected on the surface of HA sample was observed. Then the small spherical particles were obvious on the sample surfaces that would later crystallize to bone like apatite after immersion in SBF for 12 hours. After 1 day immersion, the whole surface had been covered by the precipitates and its was observed in the form of a worm like-structure, caused by the orientation of the growth process, and growing to a leaf-like structure as is shown in SEM micrographs in figure 4.6 (d-f). These layers have morphology similar to that reported in the literature [33,60]. The density of the layer rapidly increased with increasing soaking time in SBF solution. The Ca-P apatite layer on HA continuously grew to about 1.4 μm in 7 days immersion as revealed by the cross-section SEM micrograph in Figure 4.7 (a) and (b). Figure 4.7 (b) shows clearly that Ca-P layer has a deposited in interconnected pores which are similar to the surface precipitate. Additionally, the detailed morphological changes can be clearly observed on the surface of the coating using AFM as shown in Figure 4.8. The EDS analysis showed that the new layer contained calcium, phosphorus, magnesium, sodium and oxygen, whereas, in the uncovered zone or substrate, only calcium, phosphorus and oxygen were detected. The presence of Mg, Na and Cl in the EDS spectra is attributed to residual elements from the SBF solution (Figure 4.9). Compared to XRD patterns of the pure HA after immersion in SBF, the crystallinity of HA increased with increasing time but no obvious phase change was noticed in their XRD patterns. The HA phase did

remain unchanged with immersion time due to the new layer formed and starting material, having a similar compositions. After a prolonged soaking time in SBF, the intensity of the both peaks increased and became sharper, indicating the increasing amount of well crystallized Ca-P crystal (figure 4.10).

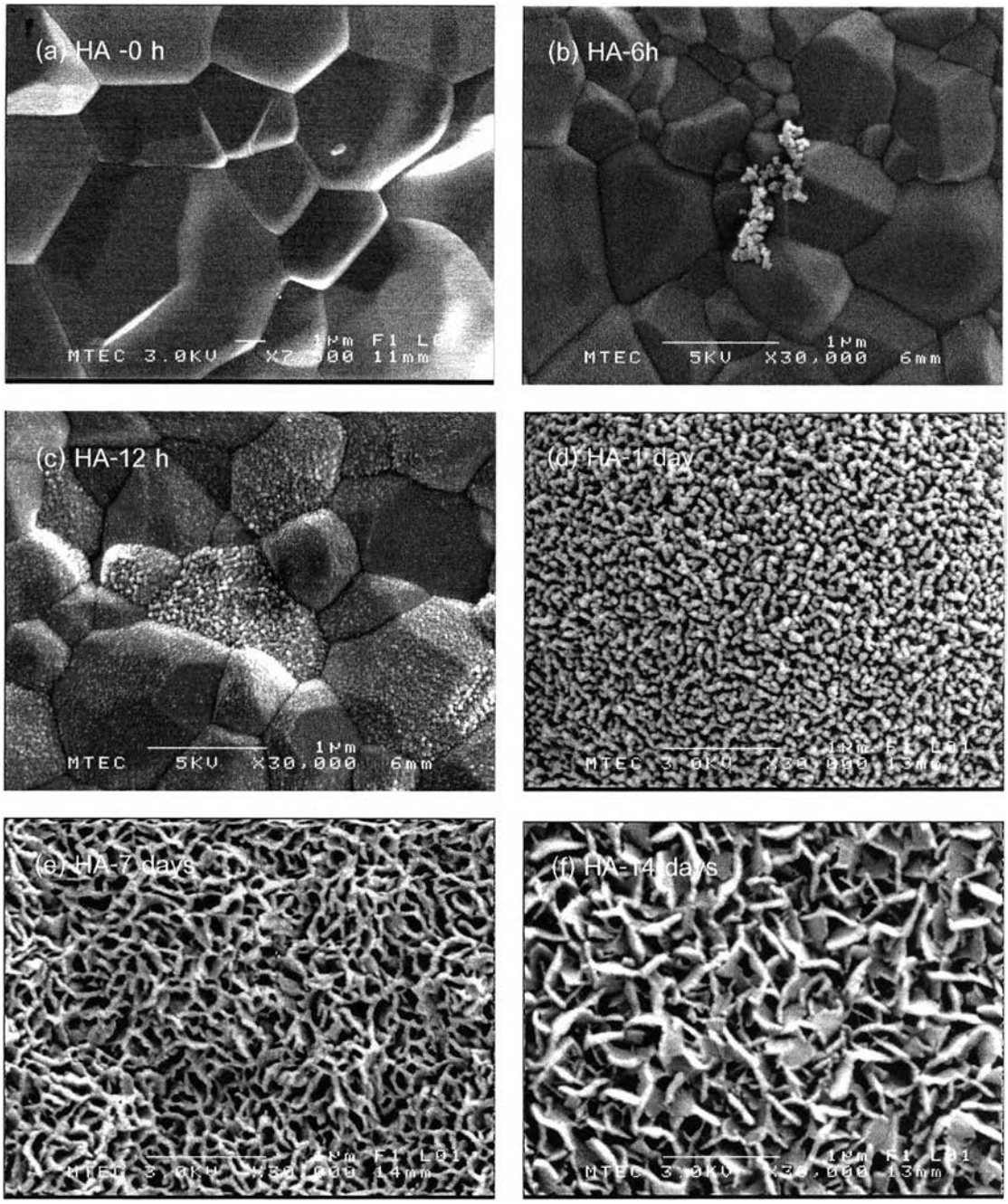

Figure 4.6 SEM images of HA without additive after soaking in SBF at 37 °C for varied periods.

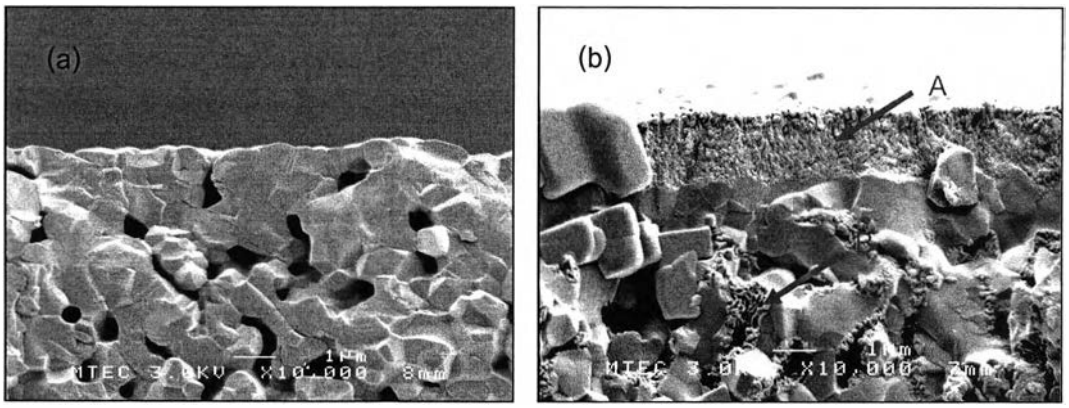

A = Ca-P layer on HA surface

B = Ca-P layer on pore HA

Figure 4.7 SEM micrographs of HA before (a) and (b) after immersion in SBF for 7 days.

Note: the growth of crystals is in the pores opening to the surface.

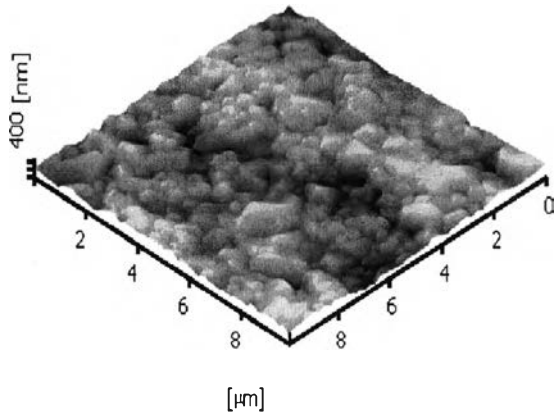

(a) HA surface characteristic before immersion in SBF

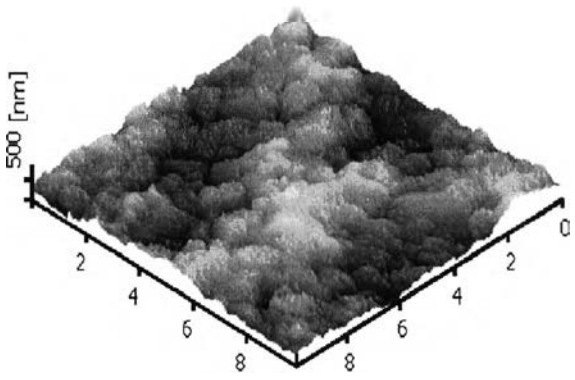

(b) Small apatite crystals depositing over the HA surface after immersion in SBF for 12 h.

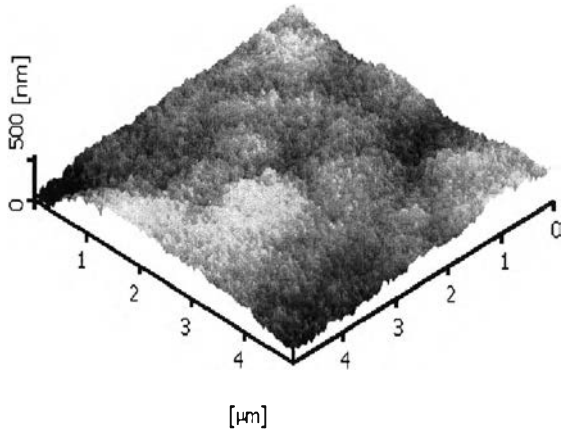

(c) Completely apatite layer cover on HA surface after immersion in SBF for 3 days.

Figure 4.8 AFM scans of the HA surface (a) before and (b) after immersion in SBF for 12 h and (c) 3 days, showing the morphological change during the early stage of HA dissolution.

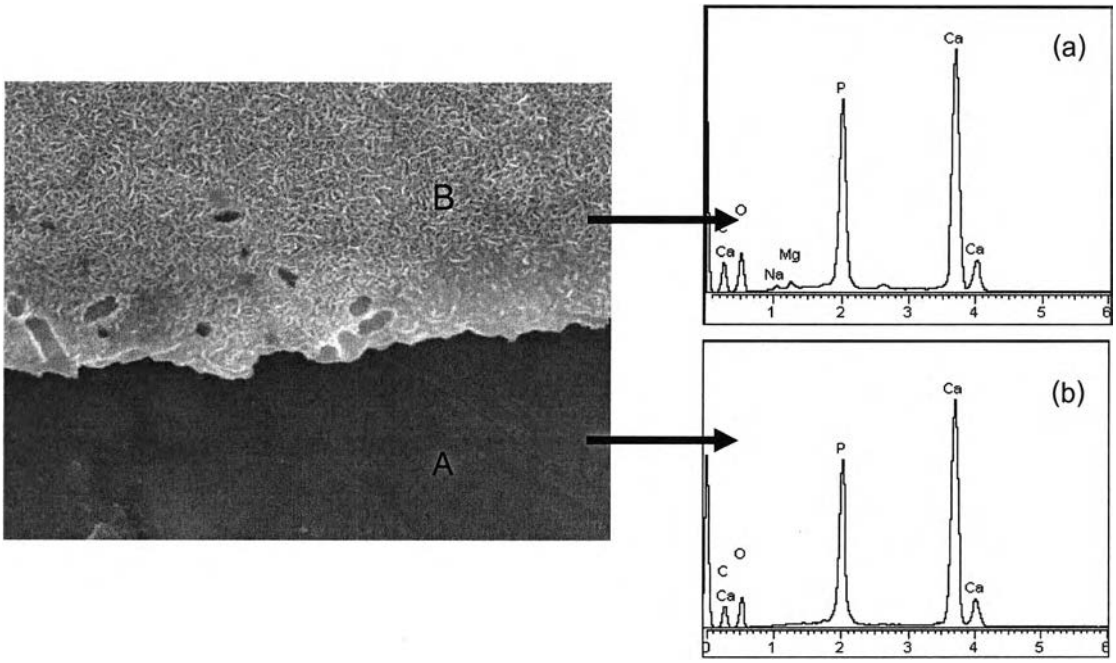

Figure 4.9 SEM image and EDS analysis of the porous HA after immersion in SBF.

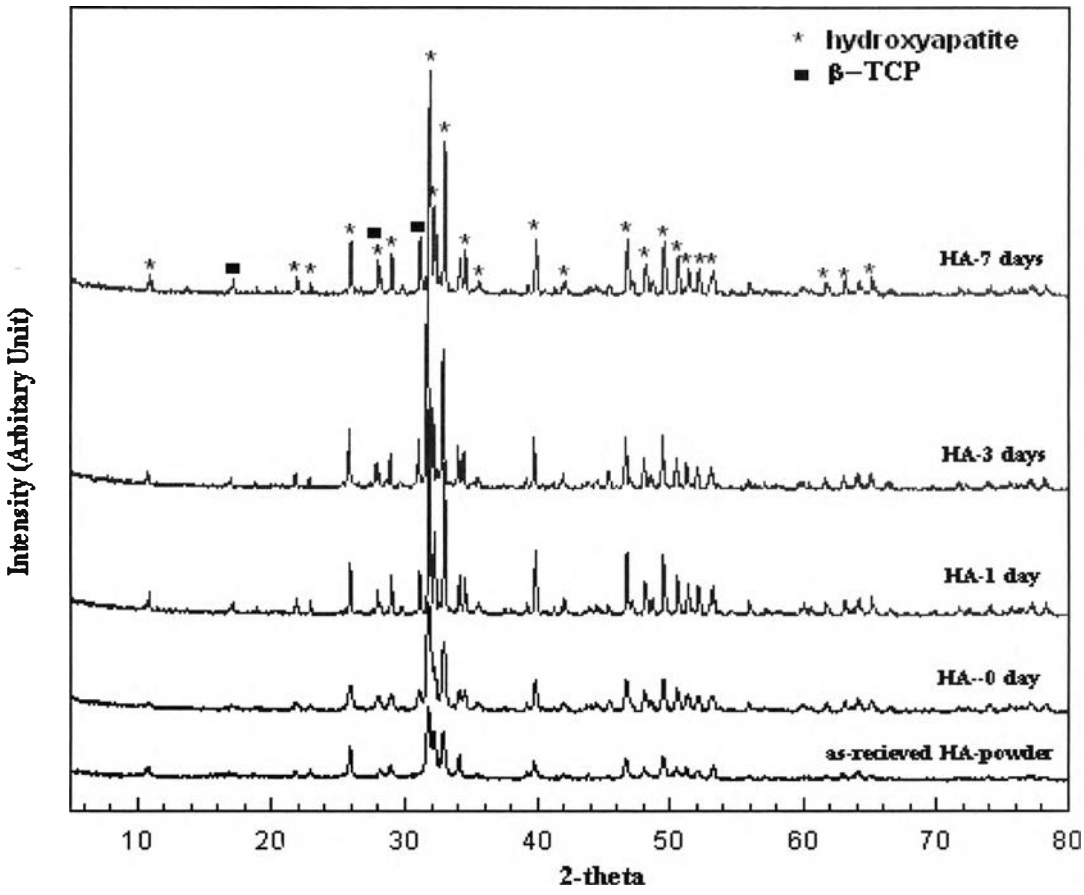

Figure 4.10 X-ray diffraction patterns of porous HA before and after exposed in SBF at 37°C.

4.2 Effect of Silica (Aerosil-200) Content on Porous HA using Uniaxial Pressing

4.2.1 Microstructure Evolution of Porous HA with SiO_2 Additive

The surface of the sintered porous HA were investigated using SEM to understand the influence of SiO_2 additive on microstructural evolution. The porous HA with SiO_2 additive was fabricated by uniaxial pressing at 14 MPa with varied additive content from 0.5 to 10 wt%. The high SiO_2 concentration was required for better density and mechanical properties of the sintered product. Above this level, slurries exhibited high viscosity due to the fine particle size and large surface area of silica powder, causing difficulty in proper mixing. Therefore, a 10wt% SiO_2 concentration was selected as highest concentration. Figure 4.11 shows the scanning electron micrographs of the surface of the pure HA and HA with SiO_2 additive. It is clear the micrographs that the porosity decreased as the silica content increased and their structure became denser due to SiO_2 particles which are joined together in as a dense agglomerate with the HA particles.

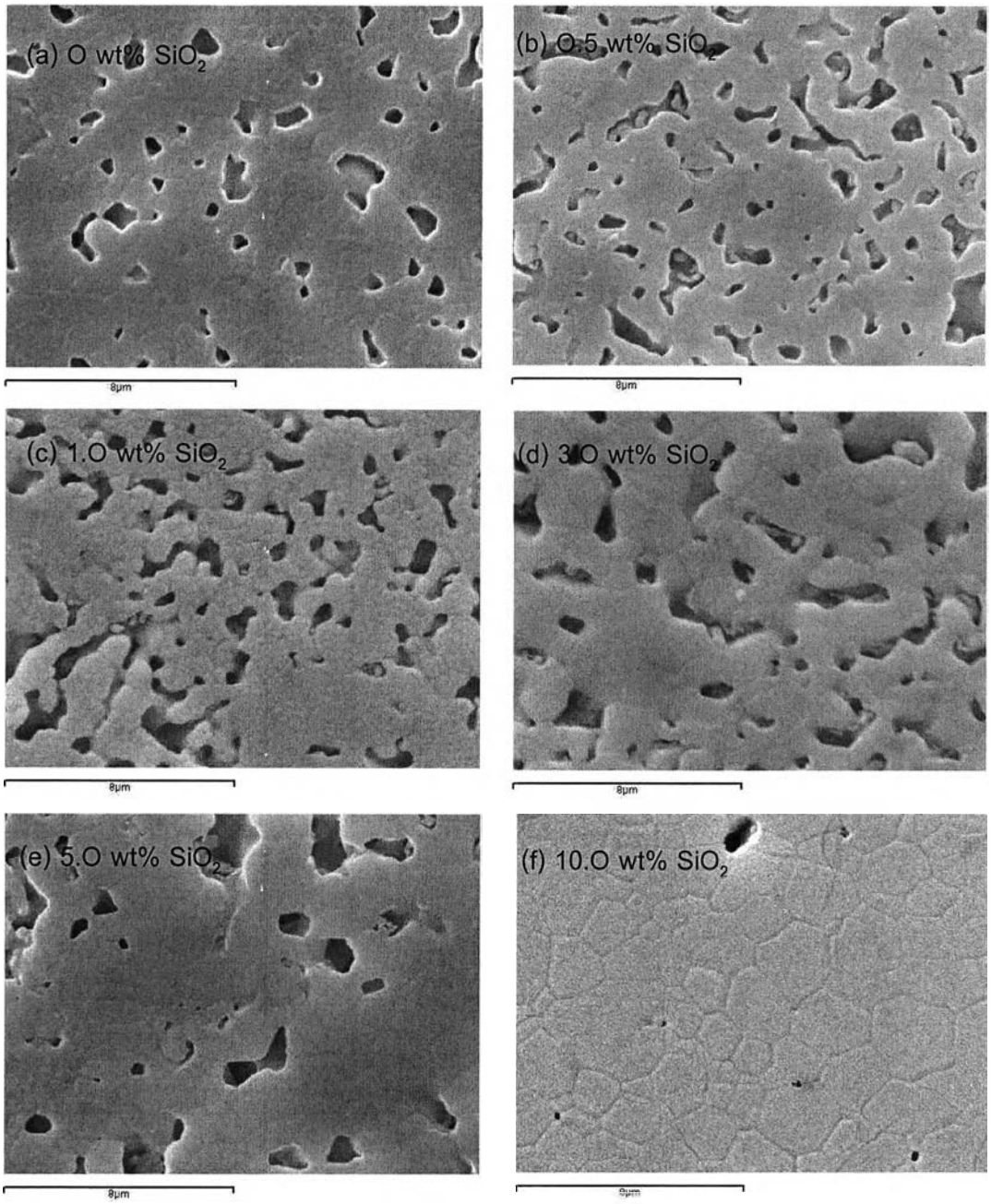

Figure 4.11 SEM micrographs of the HA without and with SiO_2 additive sintered at 1150 ^{o}C and fabricated by uniaxial pressing.

4.2.2 Phase Formation of Porous HA with SiO_2 Additive

The effect of SiO_2 on phase transformation of hydroxyapatite ceramics was observed. The XRD pattern and morphology of fumed silica (SiO_2; aerosil-200) are presented in figure 4.12. The fumed SiO_2 powder shows XRD pattern characteristic of the amorphous material. The diffraction pattern of unsintered HA corresponded with the standard HA powder diffraction file (JCPDS Card No. 09-0432). No additional phase was identified. XRD patterns of the pure HA and the mixtures of HA with different amounts of SiO_2 additive after sintering at 1150 °C for 4 h are presented in Figure 4.13. The effect of SiO_2 added in the form of Aerosil-200 fumed silica on the crystalline components of HA sample after sintering at 1150 °C was illustrated most directly by its effect on the intensity of x-ray diffraction peaks at $2\theta = 31^\circ$ and $2\theta = 31.8^\circ$. The peak at $2\theta = 31^\circ$ is solely characteristic of β-TCP and that at $2\theta = 31.8^\circ$ of HA. The intensity of the main diffraction peak for HA ($2\theta = 31.8^\circ$) decreased with increasing SiO_2 content. While, the intensity of the major diffraction peak of β-TCP ($2\theta = 31^\circ$) increased with increasing SiO_2 content. From the results it can be concluded that in the mixtures, the transformation of HA to β-tricalcium phosphate (β-TCP) took place and this reaction was higher as the SiO_2 content increased. These results are similarly increased with sintering temperature as in the previous section. At temperatures above 1150 °C, HA can become unstable and may eliminate OH^- groups from decomposed products of additional phase such as β-TCP and α-TCP. This is also confirmed by the calculated phase ratio of HA with various amount of SiO_2 in Table 4.1. Many researchers reported the presence of metal ions could help change HA to the TCP phase as the same in the present results. For example, M. Inuzuka et.al., has shown the solid state reactions between HA and ZrO_2 powders resulting in the decomposition of HA to β-TCP phase [61]. Also S. Padilla et.al [60] presented the phase transformation of HA to β–TCP and α-TCP took place with the higher amount of glass content. From the results, none of $CaSiO_3$ peaks can be found in the patterns, presumably due to the limited ability of XRD analysis. These observations differ from previous studies on the silicon substituted in HA powder in that the $CaSiO_3$ phase appeared at high silicon content [60].

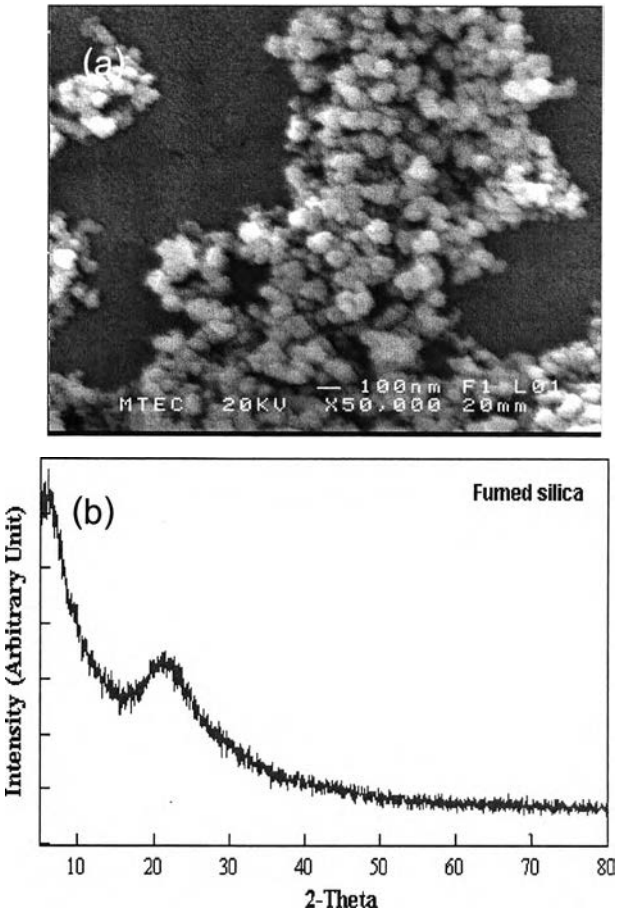

Figure 4.12 SEM micrograph and X-ray diffraction pattern of fumed silica (SiO_2; Aerosil-200).

Table 4.1 Variation of phase composition of HA with SiO_2 additive sintered at 1150 °C

	Phase ratio (%) at 1150 °C	
wt.% SiO_2	HA	β-TCP
0	88.40	11.60
0.5	70.18	29.82
1.0	59.75	40.25
3.0	22.95	77.05
5.0	17.19	82.98
10.0	11.82	88.18

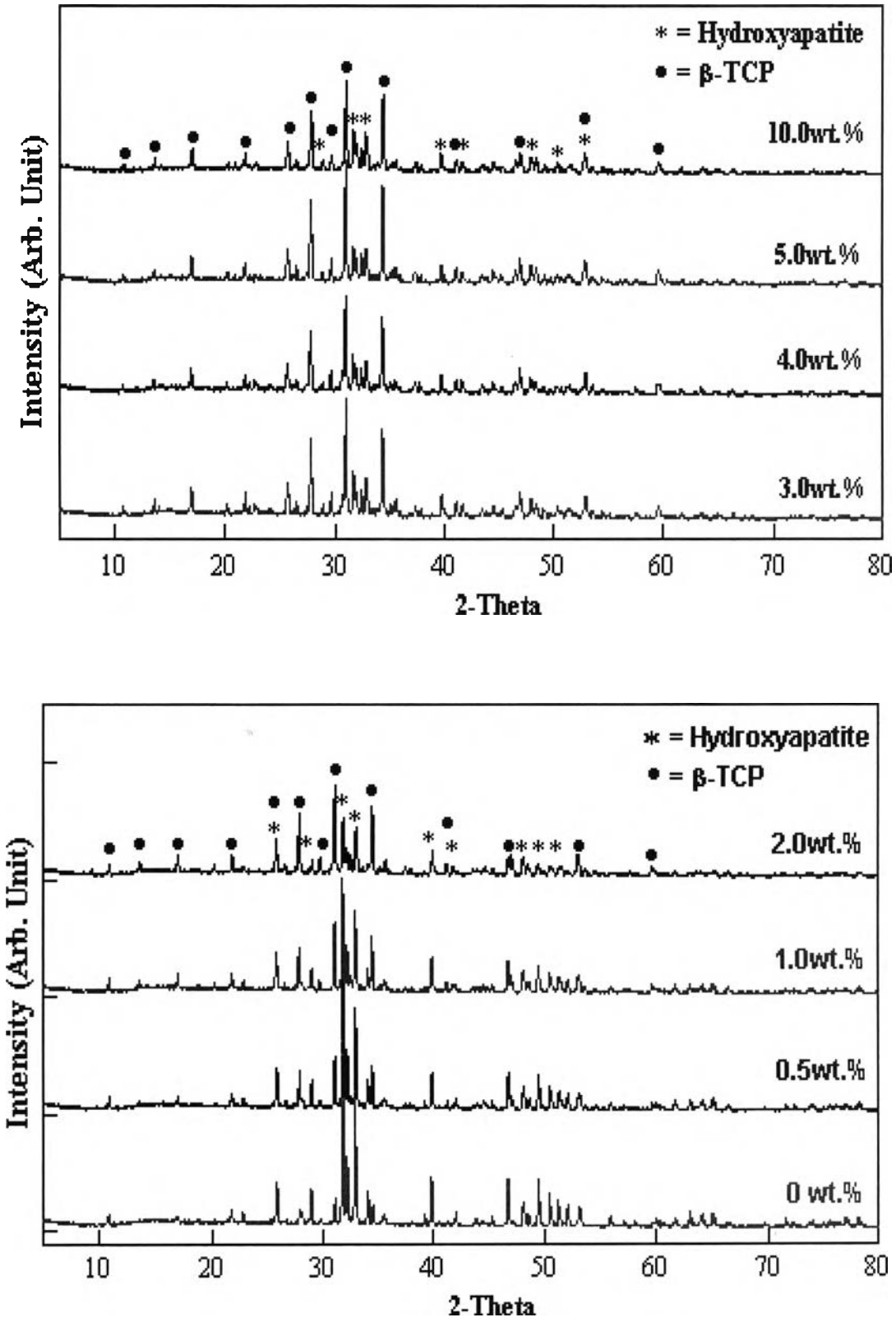

Figure 4.13 XRD patterns of HA with varies amount of SiO_2 after sintered at 1150 ^{o}C.

FT-IR spectra of fumed silica (Aerosil-200), β-TCP, and HA are shown in Figure 4.14. In the spectra of HA powder, the broad band at about 3400 cm^{-1} corresponds to the absorbed hydrate and sharp peak between 3570 and 630 cm^{-1} belong to the stretching vibration of lattice OH ions. Both these peaks are not seen in β-TCP (commercial powder) indicating the disappearance of hydrate groups in this phase. FT-IR spectra for the HA and β-TCP powder presented in this figure have indicated the vibration bands of PO_4^{3-} group at 474, 570, 601, 946-962, 1047 and 1089 cm^{-1} of apatite and TCP phase. The peaks in the region of 474, 810, 1116, 1633, 2850 and 2919 cm^{-1} represent the characteristic of silica [58]. The broad band observed at 3434 cm^{-1} is the molecular of water adsorption [46].

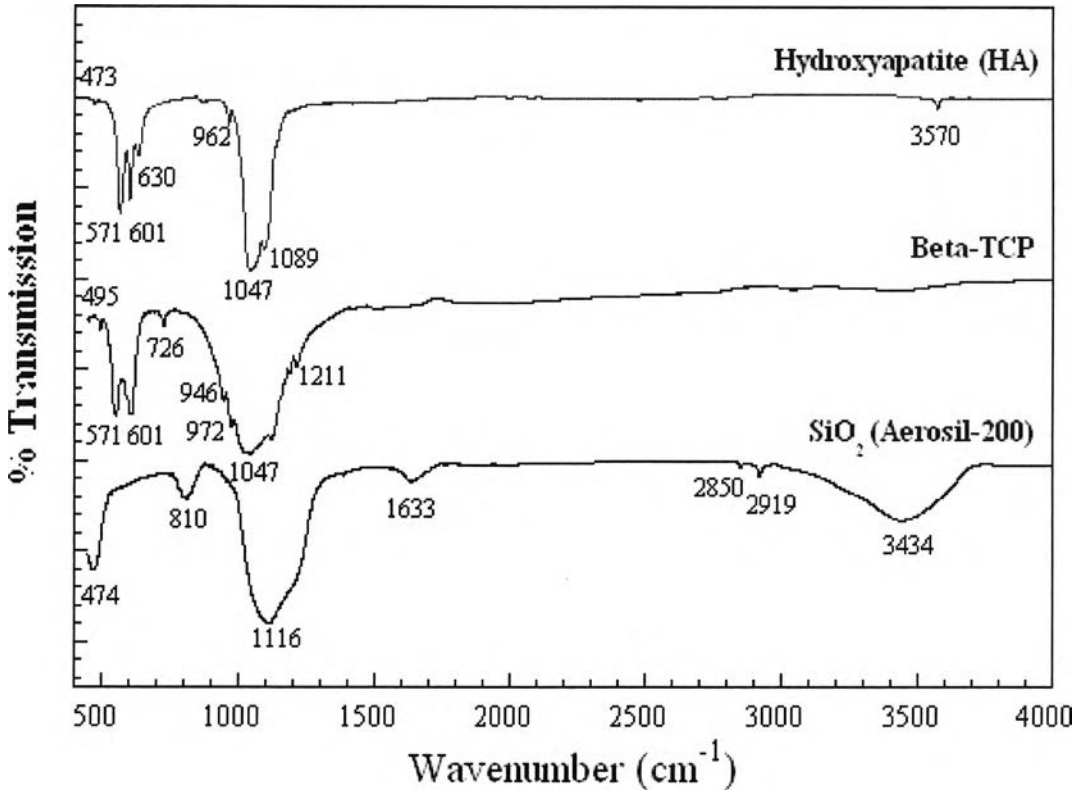

Figure 4.14 FT-IR spectra of pure HA, β-TCP and fumed silica (SiO_2; Aerosil-200).

Figure 4.16 shows the chemical functionality of HA with the SiO_2 additive sintered at 1150 °C was analyzed by the FT-IR spectra. It can be seen from the results that all the absorption peaks corresponding to the hydroxyapatite and tri-calciumphosphate phases are identified as follows. Bands at 3570 and 630 cm^{-1} indicate the presence of hydroxyl groups. Characteristic peaks of PO_4^{3-} appear at 474, 570, 601, 946-962, 1047 and 1089 cm^{-1}, respectively, and these peaks remain in the sintered samples because they are due to the core (PO_4^{3-}) group of α-TCP. Bands at 810 and 1116 cm^{-1} can be observed for the HA with silica additive at more than 4.0 wt%. From the FT-IR results, the characteristic vibration band due to OH^- groups at about 630 cm^{-1} is very sensitive to changes in SiO_2 additive content. In contrast, the band corresponding to the OH- groups stretching vibrations at about 3570 cm^{-1} is more stable as the SiO_2 additive increased. Therefore, at 630 cm^{-1} the band became small and disappeared in HA with SiO_2 doping of more than 3.0 wt%. The band at 3570 cm^{-1} can not be seen from HA with SiO_2 doping more than 3.0 wt% in Figure 4.15. The intensities at 3570 and 630 cm^{-1}, the hydroxyl stretching bands, of HA with SiO_2 samples drastically decrease with increasing amount of silica compared with those of the hydroxyapatite spectra. This can be ascribed to the OH^- sublattice of the apatite being fully occupied and the loss of OH^- ions indicate that the decomposition of HA to β-TCP has proceeded.

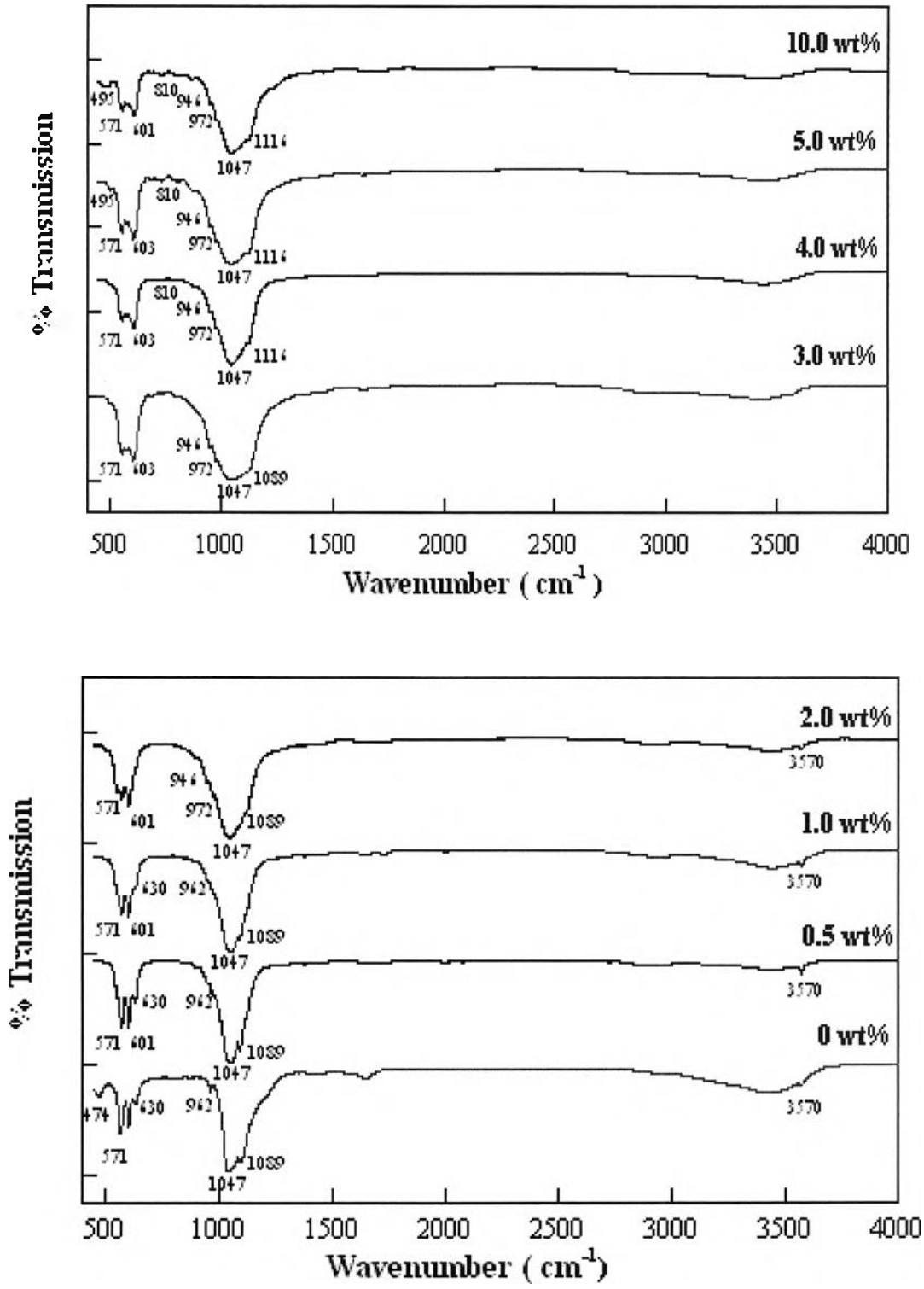

Figure 4.15 FT-IR spectra of HA with varies amount of SiO_2 additive after sintering at 1150 °C.

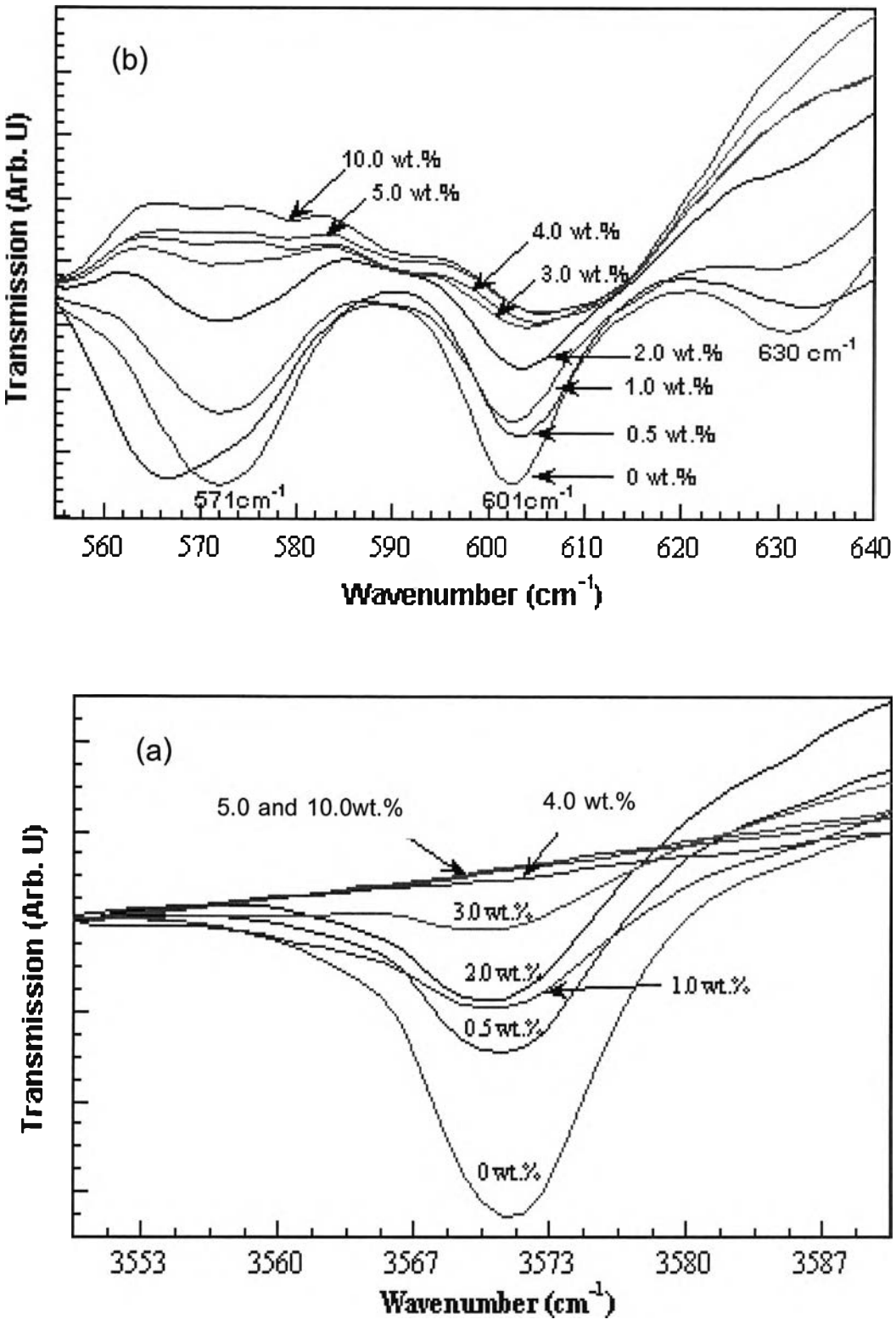

Figure 4.16 FT-IR spectra measured near (a) 3570 cm^{-1} and (b) 630 cm^{-1} as a function of SiO_2 content. This corresponds to the OH^- stretching frequency.

Figure 4.17 shows the surface morphology and chemical analysis data by energy dispersive spectroscopy (EDS) of HA with SiO_2 additive sintered at 1150 °C. It can be observed that samples present a surface commonly found in sintered materials. The main elements present in the HA powder are calcium, phosphorus and oxygen. Generally the morphology of HA with additive was similar in all material surfaces or quite homogeneously distributed, but some particles zones with a different morphology and composition were observed in Figure 4.18. Figure 4.18 HA with 5.0wt% SiO_2 doped shows small and isolated zones with different silicon contents. Silicon content in the region B was higher than in most of the remaining surface. The difference of chemical values in two distinct regions of this sample is also given in Table 4.2 for further clarification. Figure 4.19 shows the surface morphology of HA with and without SiO_2. The low magnification view of the fracture surface indicates that HA with 10 wt% SiO_2 fails in a different manner. From Figure 4.19 (c), it is apparent that the structure had surface cracks and voids in the samples, which contributed to the change in mechanical properties.

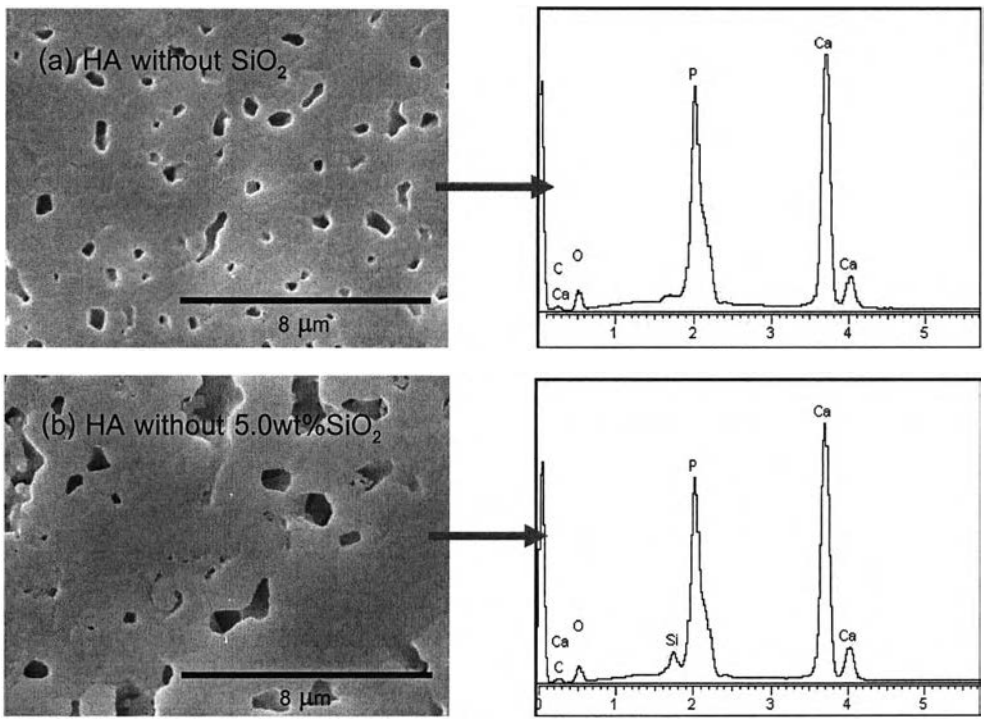

Figure 4.17 SEM images and EDS results of (a) HA without silica (b) HA with 5.0wt% silica sintered at 1150 °C.

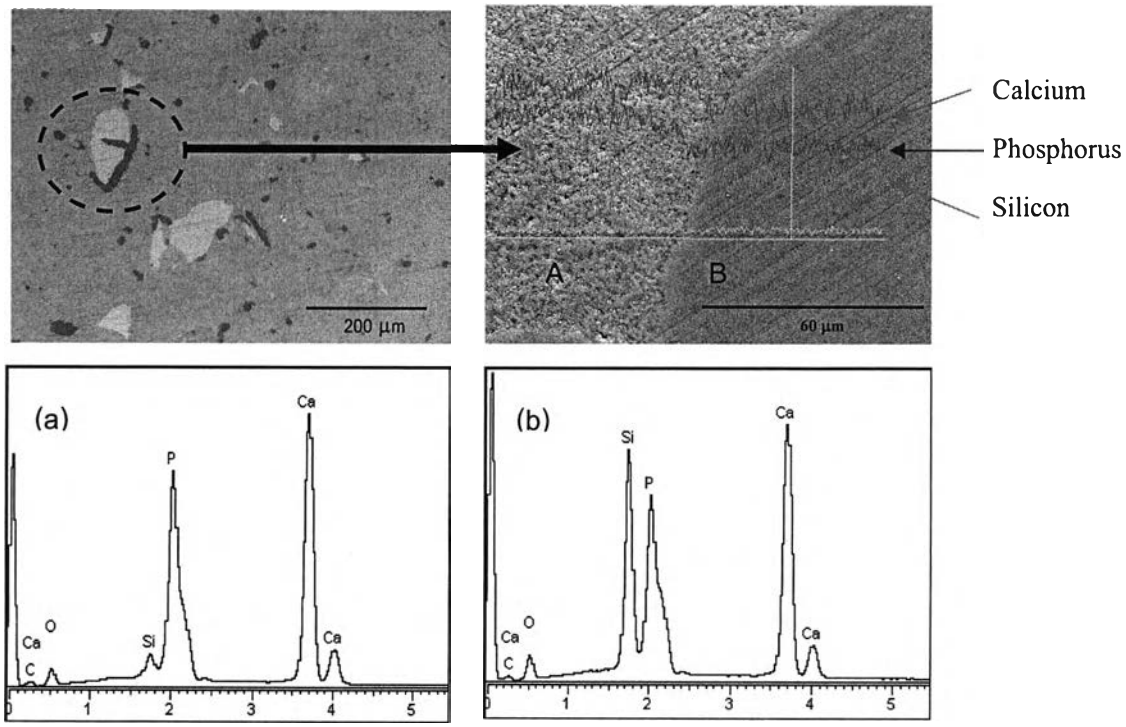

Figure 4.18 SEM images and associated EDS analysis of 5.0wt% SiO_2 – doped HA sintered at 1150 °C (Arrow indicates the selected area of the analysis).

Table 4.2 Chemical analysis data of HA with silica additive from Figure 4.18.

Element	Weight (%)		Atomic (%)	
	Area A	Area B	Area A	Area B
C	9.42	10.44	18.07	19.22
O	30.11	30.09	43.34	41.59
Si	2.18	17.29	1.79	13.62
P	19.60	14.19	14.57	10.13
Ca	38.68	27.99	22.23	15.45

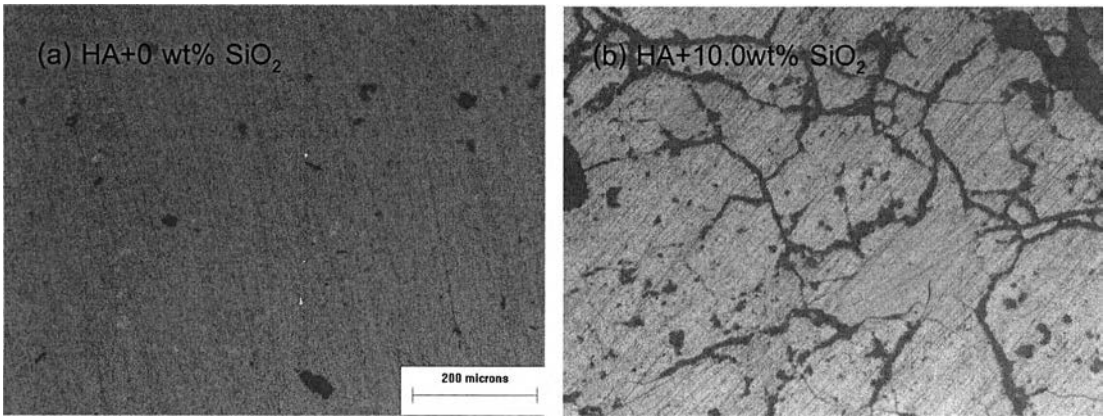

Figure 4.19 OM micrographs of the sintered HA without (a) and (b) with SiO_2 additive (10.0 wt% SiO_2) using uniaxial pressing.

4.2.3 Porosity and Density Measurement of HA with SiO_2 Additive

Five samples of each composition were used to calculate bulk densities. The value of bulk density calculated using the Archimedes techniques. The results on sintered densities of HA having different SiO_2 additive content are reported as a bar plot in Figure 4.20. The influence of additive content on bulk sintered densities for HA with 0.5 to 10.0 wt%SiO_2 additive sintered at 1150 ^{o}C for 4 hours showed improved densification for an additive content of 10wt%SiO_2. Sintered samples produced in this work exhibited bulk densities varying from 1.8 to 2.46 g/cm^3, depending on the concentration of SiO_2 added used in the fabrication process. Sintered densities measured for pure HA averaged 2.37 g/cm^3. The highest density achieved in this study was 2.46 g/cm^3 for HA with 10wt% SiO_2 additive. SEM micrographs in Figure 4.11 showed that, liquid phase sintering was achieved for 10wt% SiO_2 additive. No pores were visible even at a very high magnification for this content level, which explains why HA with 10wt% SiO_2 additive showed the maximum sintered density.

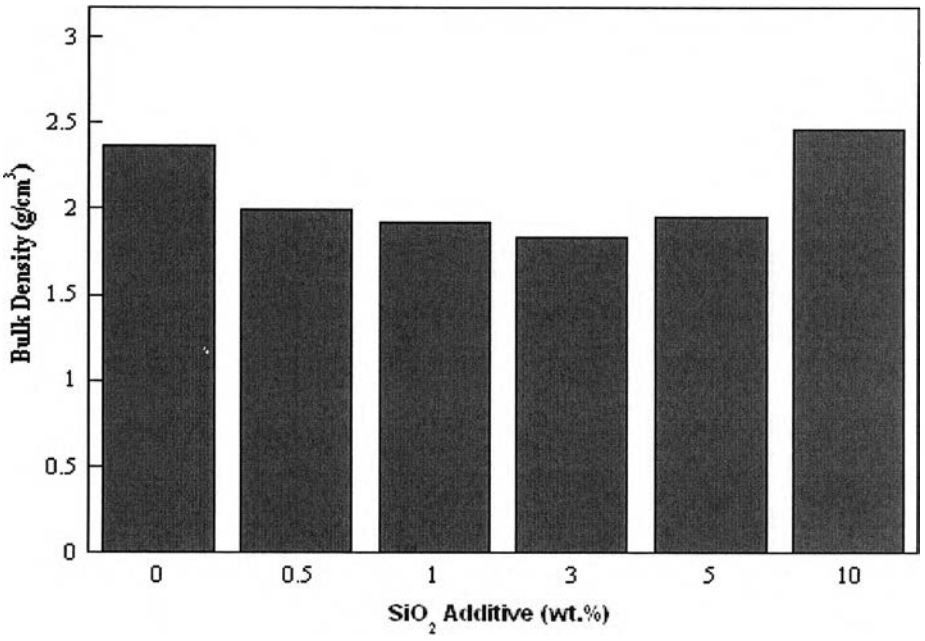

Figure 4.20 Sintered densities of HA with varied amount of SiO_2 additive sintered at 1150 ^{o}C.

4.2.4 Mechanical Properties of Porous HA with SiO_2 Additive

The compressive strength and Vicker's micro-hardness are important parameters which help define suitability of HA with SiO_2 additive for biomedical applications. Measured values are shown in Figure 4.21. HA compositions containing SiO_2 increased in strength as the amount of SiO_2 increased to 0.5 wt% SiO_2. A maximum compressive strength of 43 MPa was achieved for 0.5 wt%, after which compressive strength decreased as the SiO_2 increased above 0.5 wt%. At 10.0 wt% the properties decreased to the lowest value. The increase in strength of the 0.5 wt% SiO_2 – doped HA sample can be explained due to the combined effects of better densification and reduced grain size. The decrease in strength at 1.0 to 4.0 wt% SiO_2 is attributed to the phase transition from HA to β-TCP and increase of porosity in the composites. It indicates that the amount of porosity and phase transition play an important role on the mechanical property development. The lower strength of the 10 wt% SiO_2–doped HA sample is considered to be due to microcracks in the sample shown in Figure 4.19.

Figure 4.21 (b) shows HA compositions containing SiO_2 decreased in microhardness as the amount of SiO_2 increased up to 4.0 wt%, after which microhardness increased, at 5.0 wt% SiO_2. A maximum hardness of 342 HV was achieved for the 10.0wt% SiO_2 composition. The increase in hardness was attributed to the combined effects of better densification and reduced grain size. Also the presence of a separate silica phase at the grain boundary would enhance the hardness. A decrease in hardness due to phase transition from HA to β-TCP and increase in porosity in the samples also occurred. It is interesting to note that some of additive content showed significant improvement in compressive strength and Vicker's microhardness over pure HA. Figure 4.22 shows the typical load-displacement curves of SiO_2-doped HA sintered at 1150 ^{o}C and with varied amounts of SiO_2. It is observed that HA with SiO_2 additive less than 10.0wt%, fractured in an unstable brittle manner. This is the linear elastic region, which ends when the samples fail at maximum compressive strength. Increasing SiO_2 to more than 10.0 wt% showed a stable brittle fracture more often present in composite materials. This could be due to crack deflection and crack bifurcation resulting in the stable fracture behavior, however the larger microcracks in this sample have resulted in decreased mechanical strength.

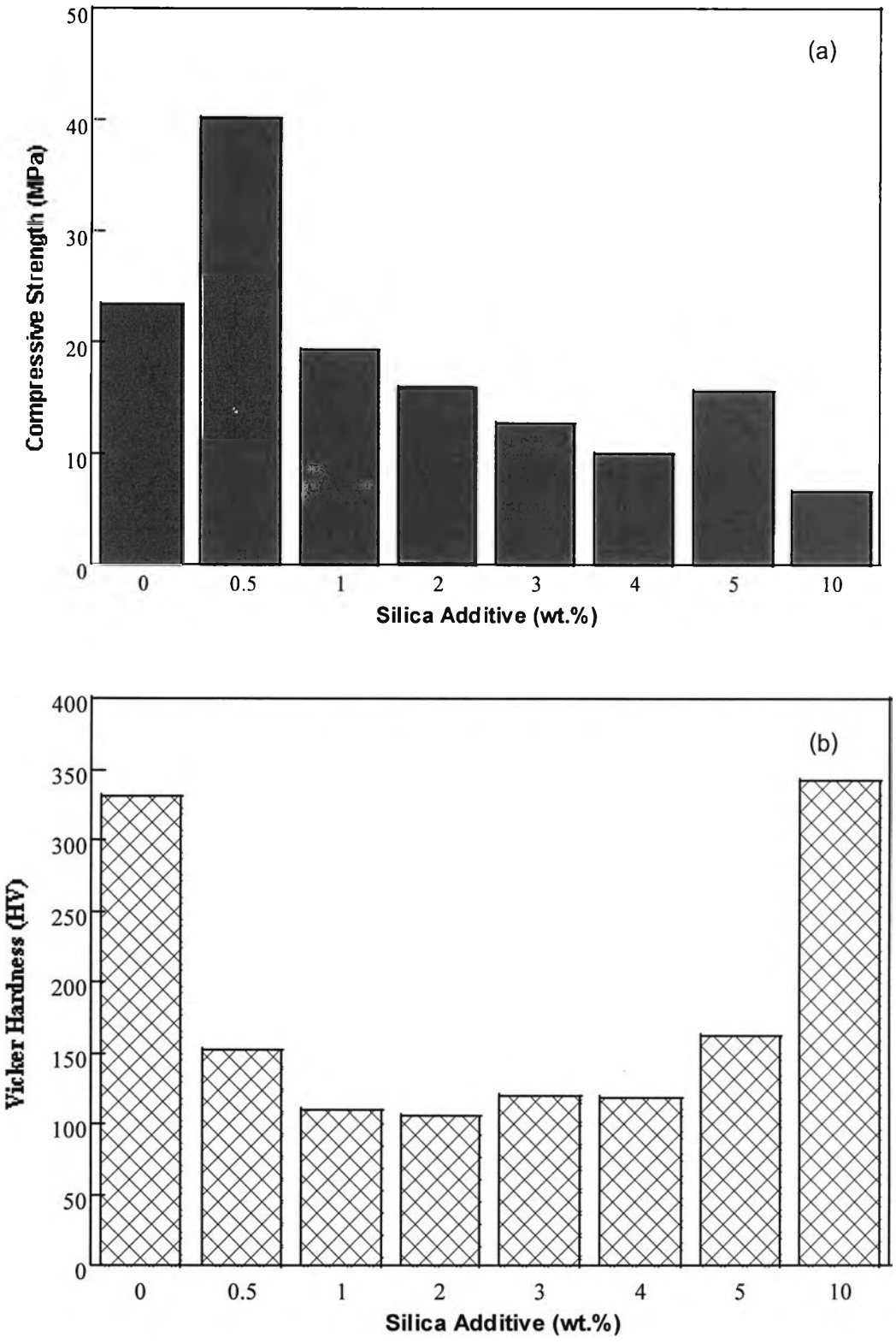

Figure 4.21 Effect of SiO_2 additives on the compressive strength and Vicker's microhardness sintered at 1150 °C.

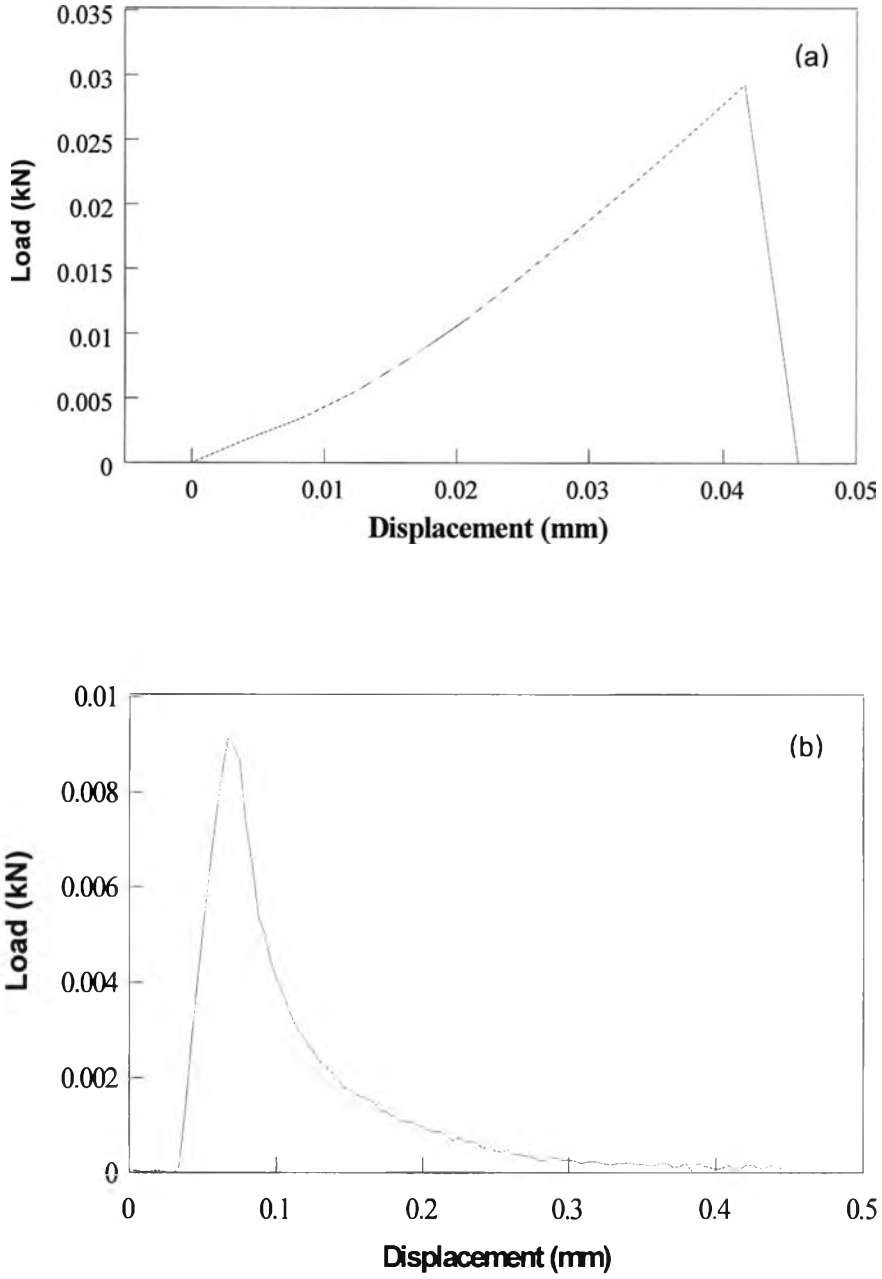

Figure 4.22 Typical load-displacement curves of the sintered HA with SiO_2 additive (a) 0.5 wt% and 10.0 wt% SiO_2.

4.2.5 *In vitro* Bioactivity of Porous HA with SiO_2 Additive

Figure 4.23 shows SEM images of HA with varied amounts of SiO_2 additive soaked in SBF at 37 °C for 5 days. With the HA doped with <5wt% SiO_2 soaked in SBF, a new layer started to form within a few days and completely covered the original surface after soaking in SBF for 5 days. The formation of the layer was rapidly increased with increasing SiO_2 additive below 5.0wt%. Acceleration of the formation of the new layer appeared to decrease with increasing SiO_2 additive above 5.0wt%. It has been reported that modification of bioactive HA by incorporating of silicon or silicate ions could enhance bone forming ability [8,18,58,60]. Low silica additive has a more open network structure that facilitates ion exchange with the solution, resulting in faster HA with SiO_2 corrosion and precipitation of apatite. Therefore, a layer of Ca-P apatite grew *in vitro* on the surface of HA with lower SiO_2 content whereas the HA sample with higher SiO_2 additive content was more resistant to corrosion and transformed slowly to Ca-P apatite due to the higher silica content that resulted in a more compact structure (high strength).

Moreover, a surface chemistry and structural basis for enhanced Ca-P apatite layer and bone formation in HA with low SiO_2 additive has been revealed in studies due to the high density of surface silanol groups (Si-OH) that exist on amorphous silica. The silanol groups in HA with SiO_2 additives tend to be more effective at inducing Ca-P layer formation than pure HA surfaces. It has been reported that Ti-OH, Zr-OH and Ta-OH groups on the surfaces could be induced apatite formation on the substrate surfaces in the body environment due it having OH groups in the end structure [1,33,56]. Therefore, the low surface area of non porous at high SiO_2 concentration and the absence of Si-OH groups limit the rate of dissolution and precipitation of Ca-P apatite on the surface. It is for this reason that increased SiO_2 contents have a decreasing bioactivity and slowing Ca-P layer formation. This result could be confirmed by E. Saiz et.al [18] who suggested that the limit of silica glass content, higher than 60 wt%, prohibited apatite layer formation on the substrate.

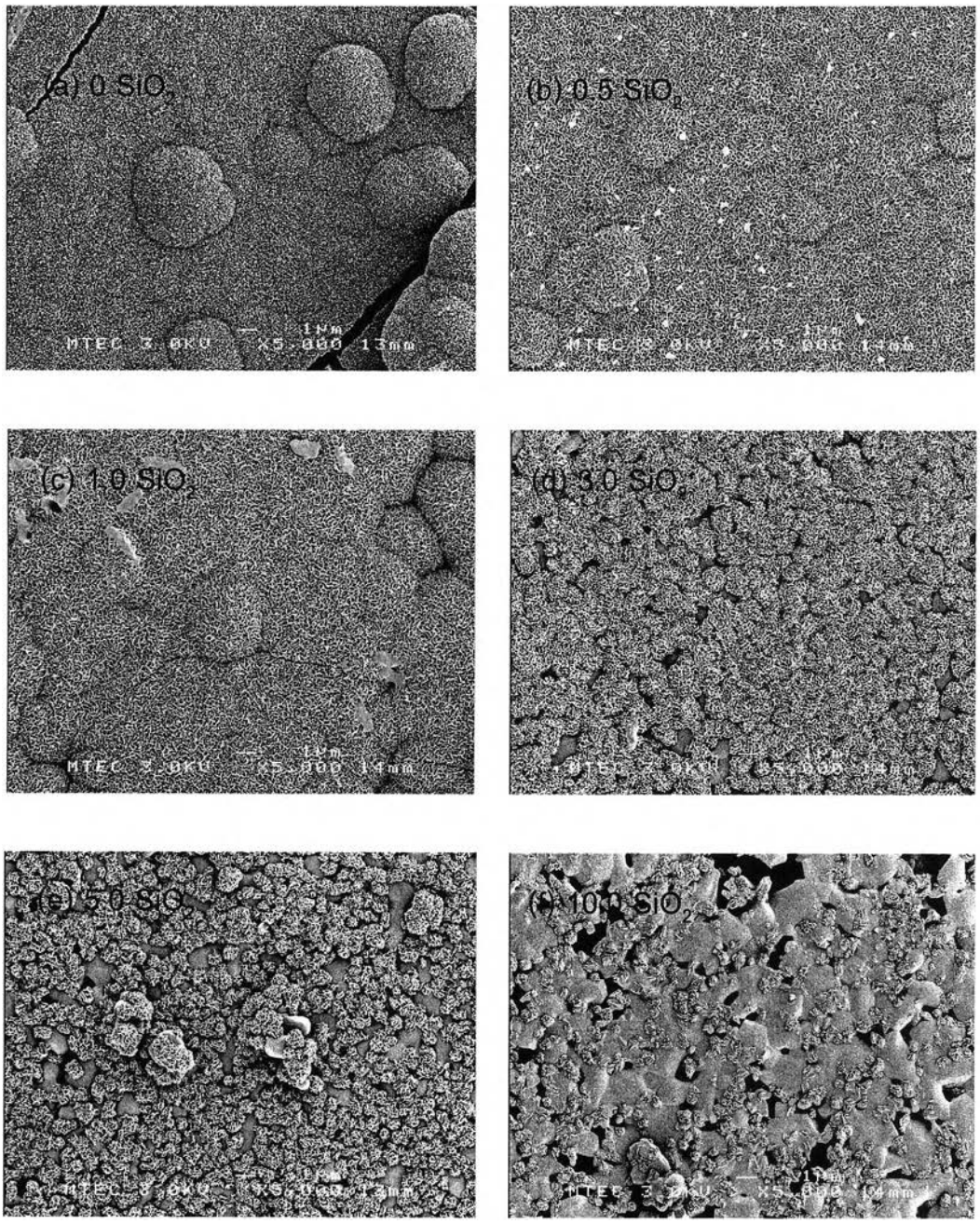

Figure 4.23 SEM images of HA with and without SiO_2 additive after immersion in SBF at 37 °C for 5 days.

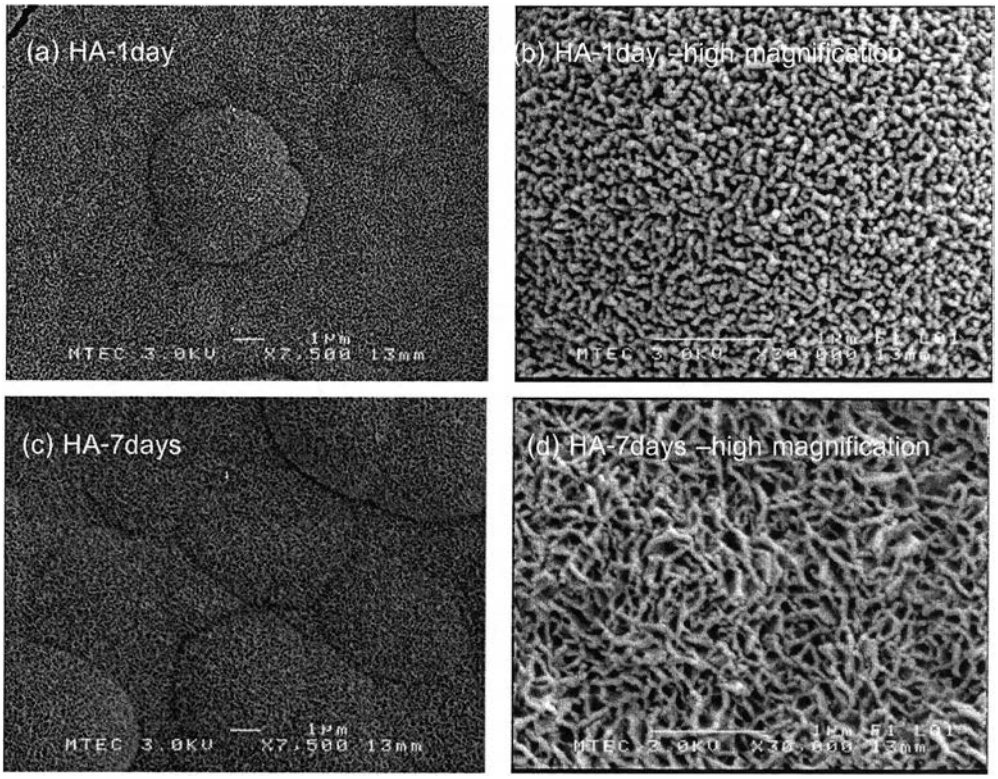

Figure 4.24 SEM images of pure HA after immersion in SBF for 1 day and 7 days and highly magnified SEM image of worm like apatite morphology.

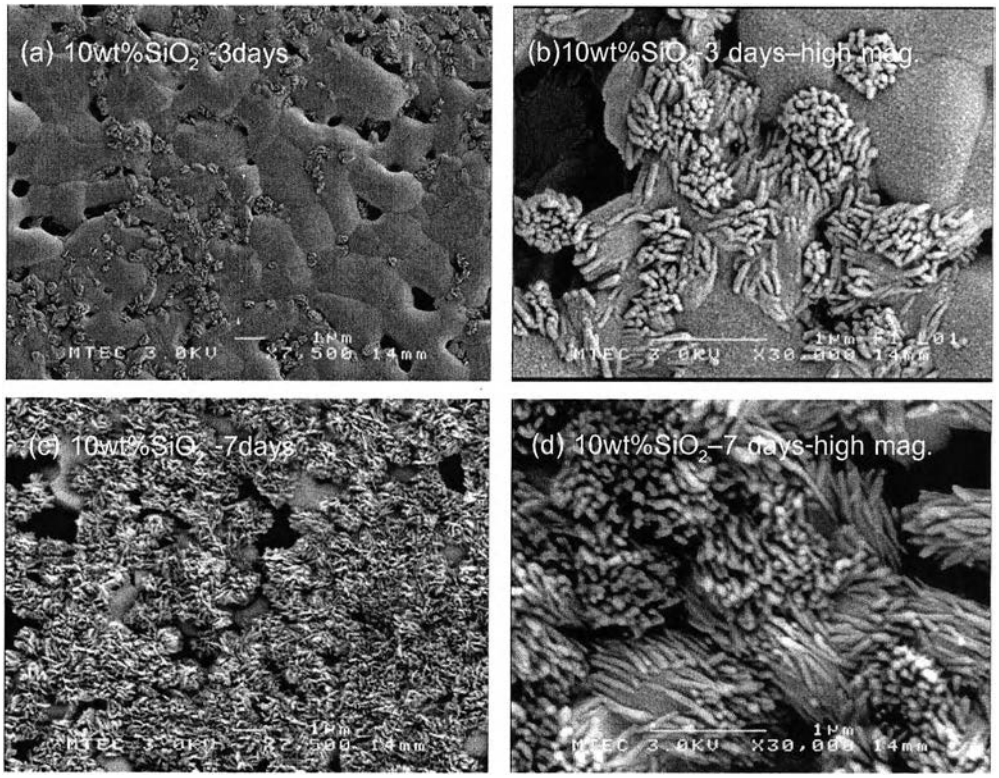

Figure 4.25 SEM images of HA with 10.0 wt%SiO_2 additive after immersion in SBF for 3 and 7 days and highly magnified SEM images of bundles of crystals.

Figure 4.24 and Figure 4.25 show the SEM images of HA with and without 10wt% SiO_2 additive after immersion in SBF. SEM micrographs showed the different morphology of the Ca-P apatite deposited on the different substrate compositions through biomimetic processing utilizing SBF immersion process. The formation of a new Ca-P layer on the surface of HA with SiO_2 lower than 5.0wt% resulted in a covering by worm-like network of crystals at the surface. After longer immersion, this could develop to leaf-like crystals, and the thickness reaching equilibrium. The surface of HA with 10.0wt% SiO_2 additive layer was composed of a lot of densely packed crystalline particles. The HA crystals growth could be observed as bundles of needles approximately 700-800 nm in length. The longitudinal direction of the needles is generally believed to be in the c-axis of the apatite crystal. A Ca-P new layer on HA with 10.0wt% silica has a similar morphology to the reported of M.H. Prado et.al [41]. They showed the morphology of HA grew in bundles of needles obtained from KOH conversion on titanium sheet.

After soaking in SBF, there was no appreciable change in the XRD pattern of HA as shows in Figure 4.26. It is similar to the XRD patterns of HA without SiO_2 additive before immersion in SBF that did not show noticeable differences, due to the similar composition of the new layer formed, within the detection limits of XRD. After a few days in SBF, the intensity of patterns obtained were much lower than that of HA before soaking in SBF, and could distinguish the new formed Ca-P apatite from original HA with additive because of the low crystallinity of new-formed Ca-p apatite. After a prolonged soaking time in SBF, the intensity of the Ca-P peaks increased and became sharper, indicating the increasing amount of well-crystallized Ca-P crystals. In a previous report, the EDS analysis demonstrated that this new layer was composed of calcium, phosphorus and oxygen similar to previous reports. No further change could be detected in the EDS analysis of the apatite layer and HA substrate after immersion in SBF for 14 days.

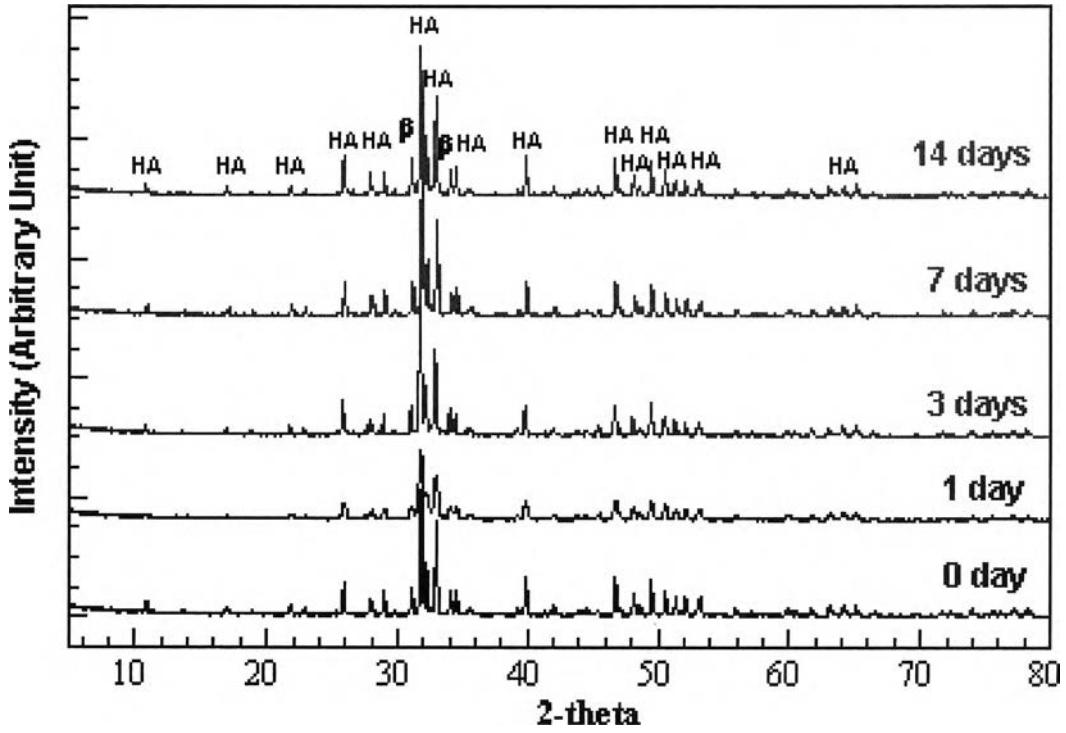

Figure 4.26 XRD patterns of HA with 0.5wt% SiO_2 additive soaked in SBF for various periods.

4.3 Effect of Glass Frit on Porous Hydroxyapatite Using Uniaxial Pressing

From the previous study of the effect of silica on porous HA, the compressive strength of porous HA decreased with increasing silica content due to the appearance of cracks on the surface of HA with high silica content. Cracking on the surface has resulted in a decrease of compressive strength. While, HA with SiO_2 additions have excellent in vitro bioactivity, since it could be induced by the formation of a precipitate layer on its surface after immersion in SBF, even for a short soaking time (less than 1 day). Therefore, the aim of this section was to study the effects of silica in the form of glass frit, on mechanical and bioactive properties of porous hydroxyapatite.

4.3.1 Microstructural Evolution of Porous HA with Glass Frit Additive

The morphology and grain size of as-received HA powder and glass frit are shown in Figure 4.27. The powder particle size of the HA is in the nano-meter range. Figure 4.28 shows SEM micrographs of the sintered HA with and without glass additive sintered at 1150 and 1300 °C. Pure HA sintered samples exhibited a grain size trend with increasing temperature, the grain size of HA rapidly increasing with sintering temperature. The addition of glass to the microstructure of HA can be seen to have caused changes and the grain size of HA has become smaller and some grain growth at higher temperatures (1300 °C). In addition, with more than 10.0 wt% of glass addition, the grain size of HA becomes more uniform and the number of pores at the grain boundaries decreased due to the trapping of pores within grains, as a result of grain growth. From such microstructural observations, it can be concluded that adding glass to HA sintered at 1300 °C results in a decrease in porosity and also grain size. The grain size of HA with the glass additive is smaller than that for pure HA. These results clearly demonstrate another useful advantage of glass frit additive in preventing grain growth when sintering at high temperature. This is important, since materials with smaller grain size would normally result in enhanced mechanical properties when compared to HA without additives sintered at the same temperature but having a larger grain size.

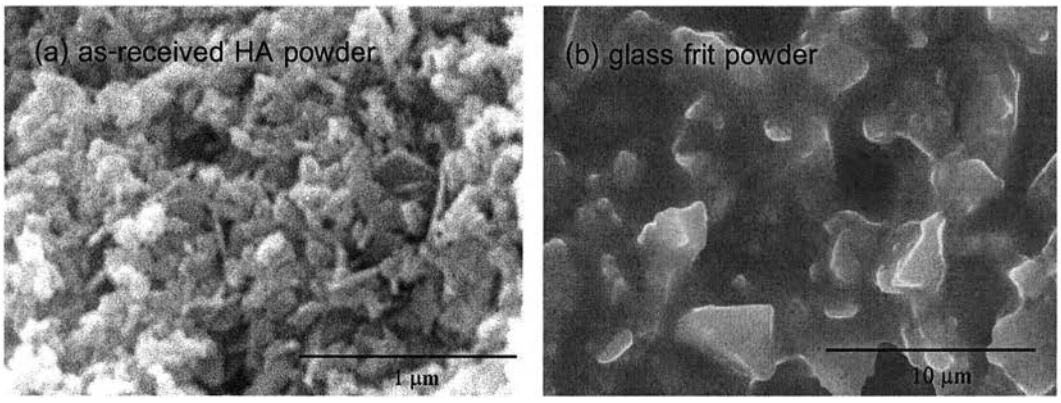

Figure 4.27 SEM micrographs of (a) HA and (b) glass frit additive powders.

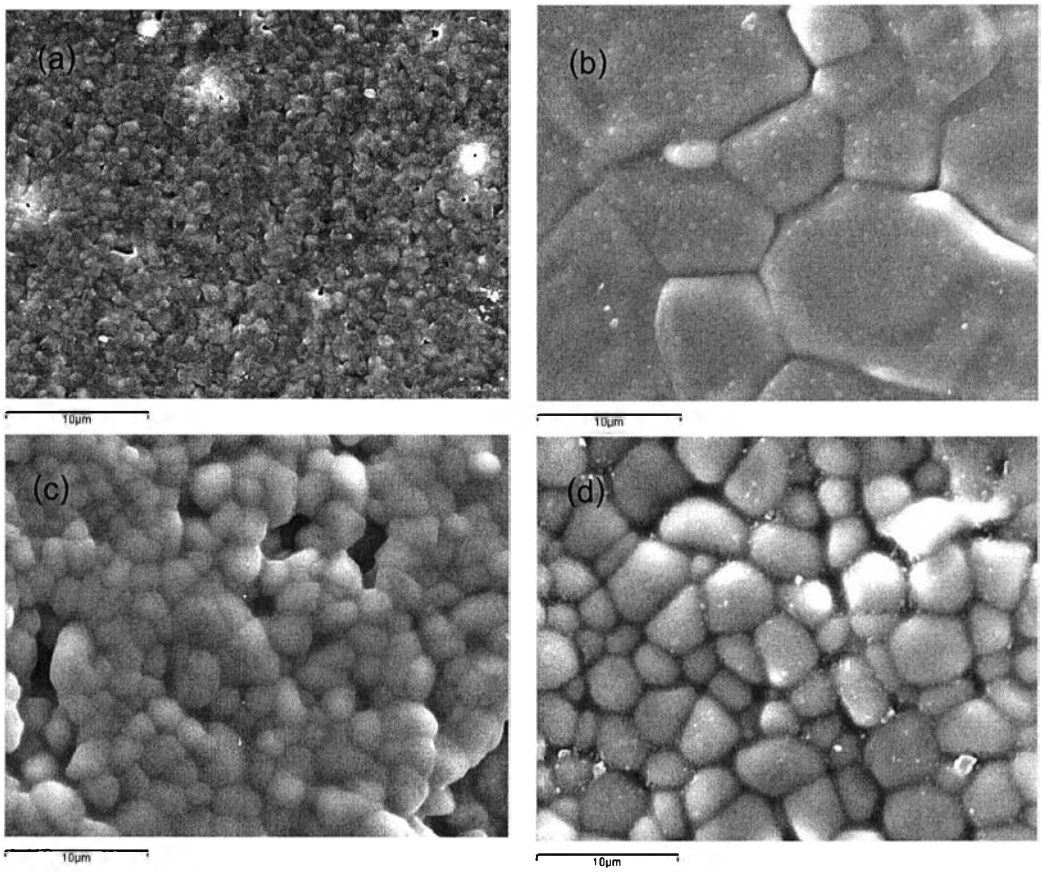

Figure 4.28 SEM micrographs of the sintered HA without additive, sintered at (a) 1150 °C, (b) 1300 °C and (c-d) HA with glass additive (20.0 wt%) sintered at 1150 and 1300 °C, respectively.

4.3.2 Phase Formation of Porous HA with Glass Frit Additive

XRD patterns of the used HA powder before and after sintering are shown in figure 4.29, the crystallinity of HA was identified by corresponding to a hydroxyapatite phase (JCPDS 09-0432). The glass frit additive (Frit no.7406) showed the typically amorphous characteristics of a glass. However, after sintering at 1150 °C and 1300 °C, XRD peaks of the sintered HA reveal the formation of β-TCP phase (JCPDS 09-0169). When the HA powder was sintered at 1150 °C for 4 h, the compositions of mixed phases were 88% HA and 12% β-TCP, and at 1300 °C there was a mixture of 82% HA and 18% β-TCP phase. This demonstrates that at higher sintering temperature, it is possible to

form β-TCP phase and the degree of conversion to β-TCP increases as the temperature of the reaction is increased. Figure 4.30 shows the XRD patterns of the sintered samples having various amounts of the glass additive. Characteristic peaks of hydroxyapatite and β-TCP can be observed in the HA with as little as 1.0 wt% added glass. Within the range of compositions employed, the XRD peaks of the HA became broader with the increasing amount of glass present. This indicates that the crystallinity of the hydroxyapatite decreases with increase in the amount of the glass additive. The peak intensity of β-TCP increased with the amount of the glass additive and the hydroxyapatite peak decreased. Additionally, no calcium silicate peaks were identified in the XRD spectra taken on the HA with SiO_2 additive. This suggests that silicon in glass forms a substituted phase within the phosphate lattice. Furthermore, this result could be confirmed by FT-IR analysis. This same tendency is observed for HA with SiO_2 additive samples as previous reported which according to the literature indicates that the transformation of HA to TCP phase occurs by incorporating additives such as ZrO_2, SiO_2, and the other elements in HA ceramics [8,58].

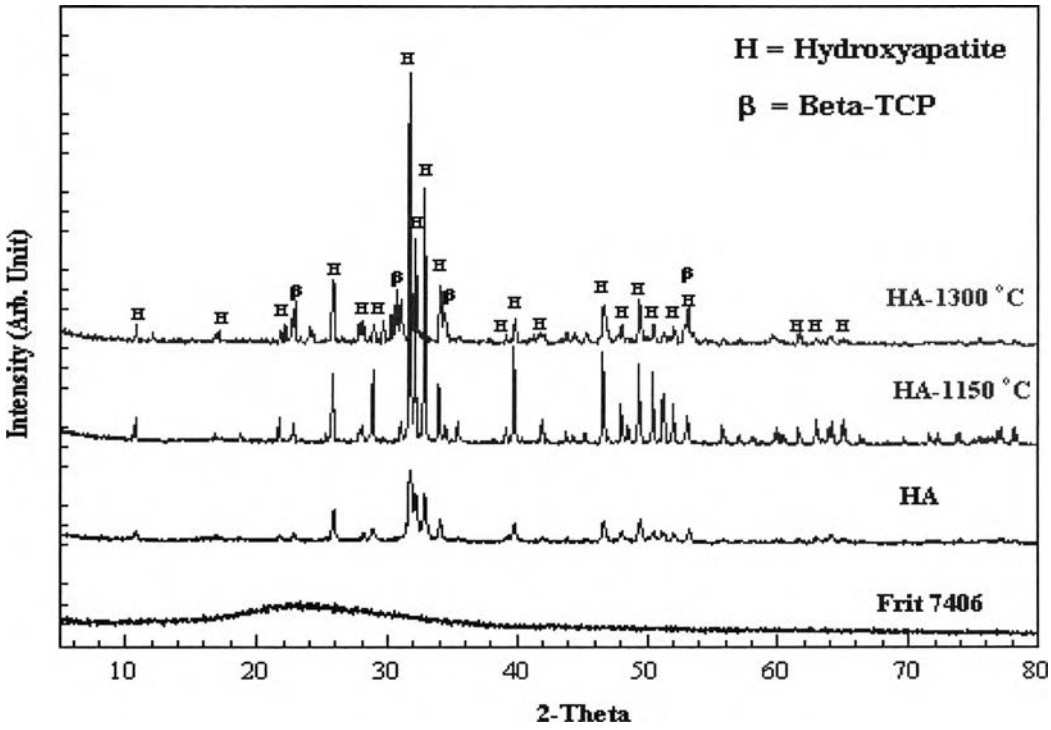

Figure 4.29 Comparison set of XRD patterns of glass frit additive, HA powder before and after sintering at 1150 °C and 1300 °C, respectively.

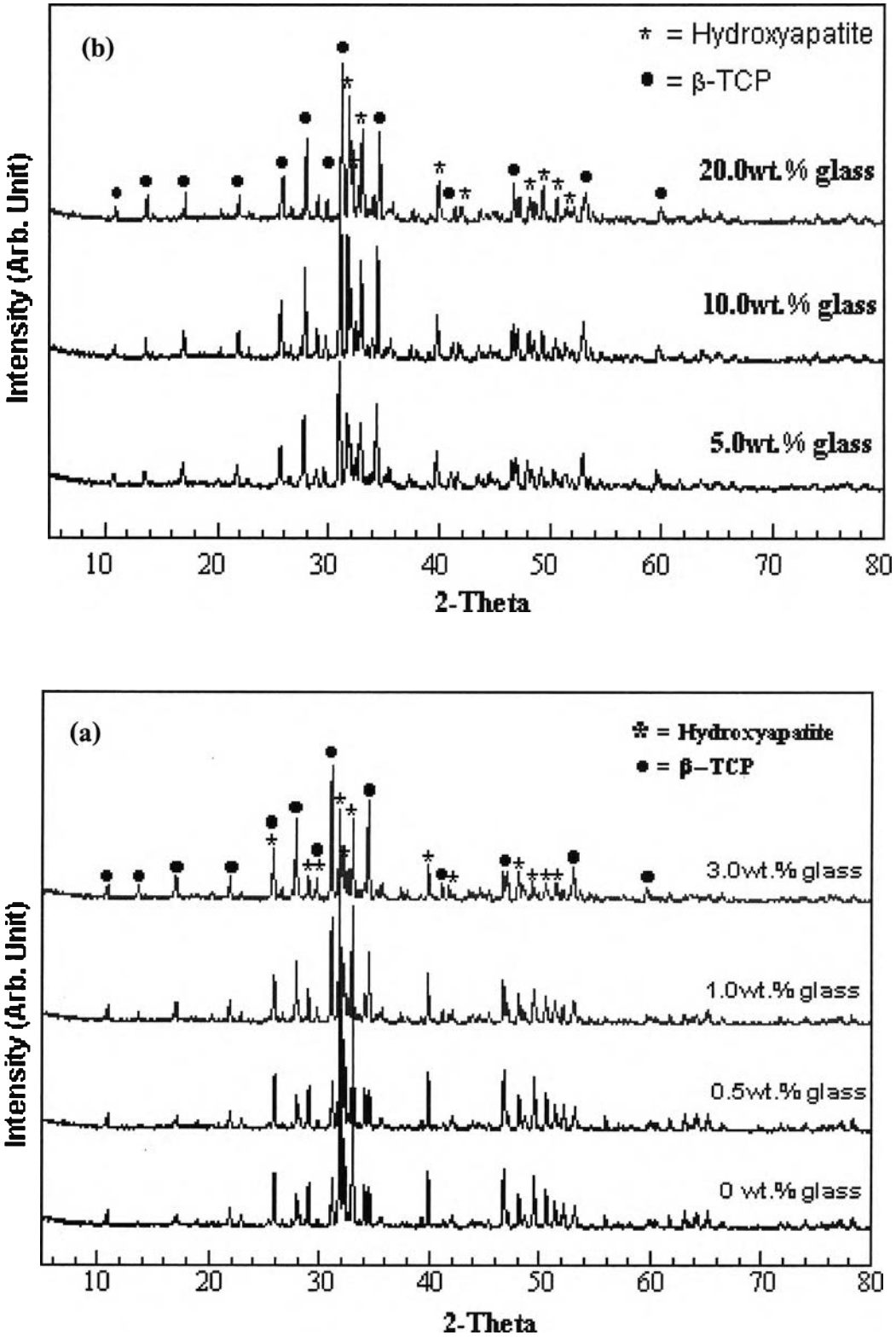

Figure 4.30 XRD patterns of HA without and with glass frit additive after sintering at 1150 ^{o}C.

4.3.3 Porosity and Density Measurement

The influence of glass addition on densification of HA at levels of 0.5 to 20.0wt% and compared with pure HA was measured by the Archimedes's method (Figure 4.31). In general, the bulk density variation of the HA samples sintered was found to increase with increasing temperature and additive content. The sintering temperature and the bulk density of glass additive have slightly decreased with increasing amount of additive from 0-3.0 wt%. The lowest density of 1.80 g/cm^3 was achieved for HA with 3.0wt% SiO_2 additive sintered at 1150 ^{o}C, after which the density increased as SiO_2 levels increased above 5.0wt%. The bulk density values of HA with 20.0 wt% sintered at 1150 and 1300 ^{o}C are 2.23 and 2.75 g/cm^3 , higher than the other composition with doping glass additive at the same temperature but slightly less than pure HA.

4.3.4 Mechanical Properties of Porous HA with Glass Frit Additive

Figure 4.32 and 4.33 show the compressive strength and micro-hardness of HA and HA with the glass additive, after sintering at 1150 and 1300 ^{o}C. Clearly, when the amount of the glass additive was increased from 0-5.0 wt%, the compressive strength has decreased. However, when the amount of additive is greater than a value of approximately 4.0 wt%, the compressive strength increases to 35 MPa at for the 1150 sample and the highest compressive strength is found for the 1300 ^{o}C (68 MPa) sample. The micro-hardness increased to 520 HV at this same sintering temperature. It can be concluded that the compressive strength and micro-hardness are dependent on sintering temperature and glass additive content.

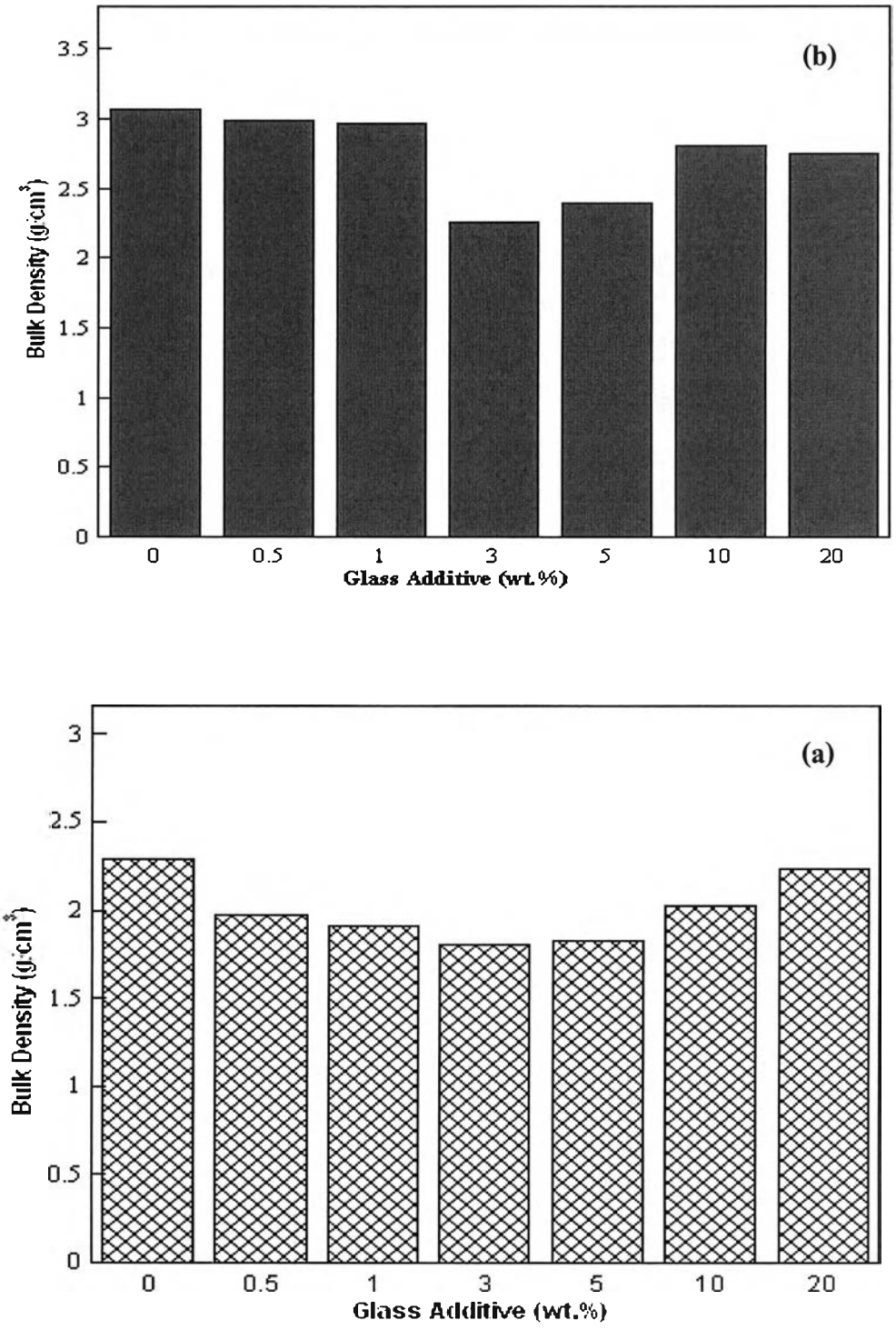

Figure 4.31 Densities of HA without and with varied amount of glass frit additive sintered at (a) 1150 °C and (b) 1300 °C.

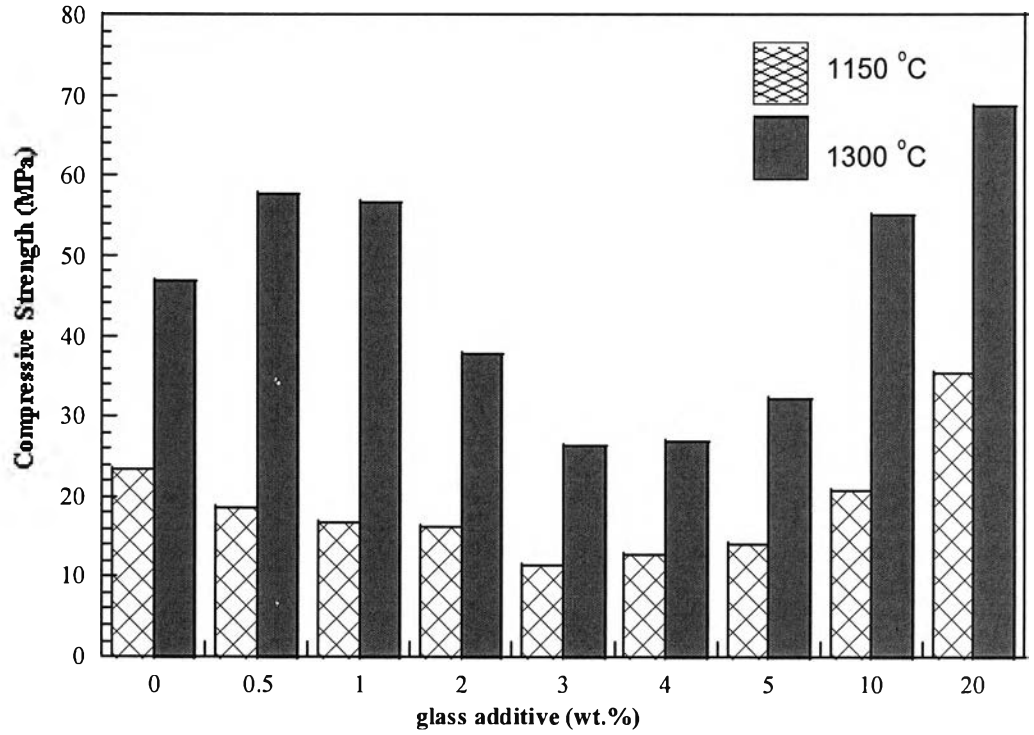

Figure 4.32 Compressive strength of the HA samples sintered at 1150 °C and 1300 °C with and without different additive content.

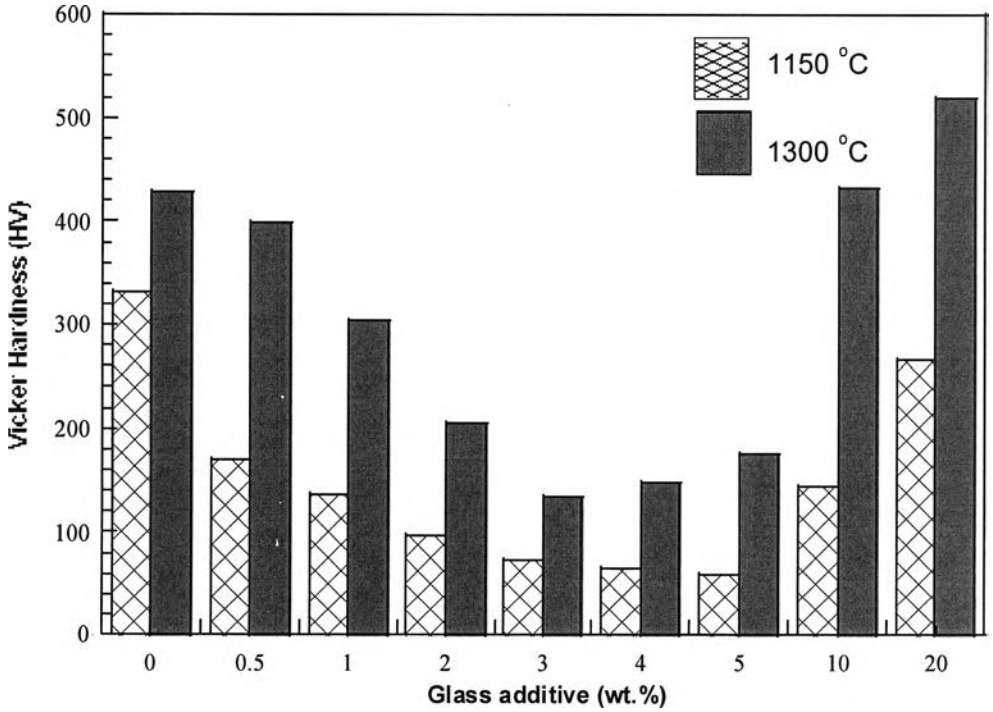

Figure 4.33 Vicker's microhardness of the HA samples with varied amounts of glass content sintered at 1150 °C and 1300 °C.

4.3.5 *In vitro* Bioactivity of Porous HA with Glass Frit Additive

Figure 4.34 shows SEM images of HA with and without glass frit additive after immersion in SBF at 37 °C for 7 days. The formation of the Ca-P layer on HA with additive surface was rapidly increased with increasing glass additive below 5.0wt%. When the amount of glass additive was increased from 0-5.0 wt%, the formation of Ca-P layer had increased. When the amount of additive is higher than a value of approximately 5.0 wt%, the acceleration of the formation of new Ca-P layer slightly decreased. The fastest formation is found at 3.0 wt% glass additive. HA ceramics with low glass additive have a more open network structure that facilitates ion exchange with the solution, resulting in faster HA formation with glass additive corrosion and precipitation of Ca-P apatite layer. As a result a layer of Ca-P apatite grew on the surface of HA with lower glass content whereas HA samples with higher glass additive content were more resistant to corrosion and slower to form Ca-P apatite due to their higher silica content that resulted in a more compact structure (high strength). According to previously reported work a significant characteristic of bioactive materials has been their ability to bond with living bone through the formation of an apatite interface layer on the surface both *in vitro* and *in vivo*. Therefore, the present study shows that the HA with glass additive induced the precipitation of a Ca-P apatite layer on its surface in SBF even for a short immersion time, which established the high degree of bioactivity of the sample.

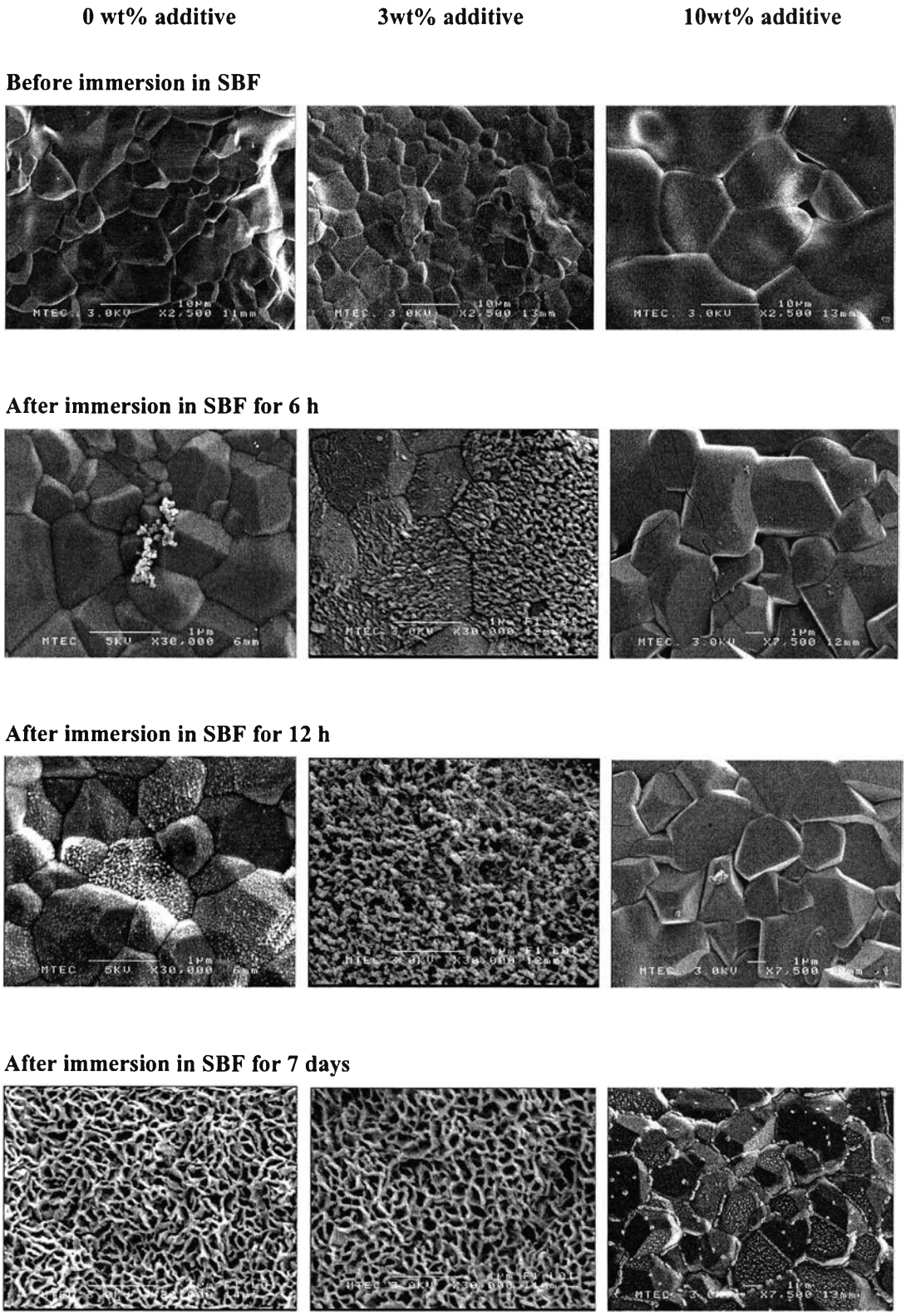

Figure 4.34 SEM images of HA with and without SiO_2 in glass frit additive after immersion in SBF at 37 °C for 7 days.

4.4 Preparation Porous HA with and without Glass Frit Additive by Polymeric Sponge Method

According to the literature, HA ceramics in porous form (porosity up to 60%) have been widely used successfully as bone substitutes. In general, it is perceived that the pores provide a mechanical interlock leading to firmer fixation of the material. In addition, bone tissue grows well into the pores thus increasing the strength of the HA implant [19]. Therefore, this work was to study and fabricate a bioactive porous HA with glass frit additive by the polymeric sponge method. This method is the common technique for fabricating porous ceramics with high porosity, highly interconnected pores, uniform pore size distribution, controllable porous structure of ceramics and it is suitable for commercialization in term of simplicity and low cost. The pore structure (e.g. porosity, pore size and degree of connection) and mechanical properties of the samples from this method were investigated in order to evaluate the possibility of using these materials as bone replacement.

4.4.1 Microstructure of Porous Hydroxyapatite

The porous ceramics were prepared with the use of polymer sponges infiltrated with HA slurries. Polymer foams from waste polyurethane foam, used for the study had high porosity and highly interconnected pores. Figure 4.35 shows the polyurethane foam with a maximum pore size of 700 μm as an example. When the foams were immersed in the HA slurry, the ceramic particles carried by the aqueous solution were able to coat the strut of the polyurethane foam. During the firing step, the struts of the polyurethane foam experienced thermal expansion, melting and evaporation. Since the HA particles were joined together due to the sintering reaction, the porous HA would not be damaged by the removal of the polyurethane foam, resulting in intact HA porous bodies. Additionally, the polyurethane foams were used to create porosities in the porous HA ceramics after firing. Therefore, the microstructure replicates the porous structures of polyurethane foams, these serving as polymer templates. The different

pore size and geometries can be achieved by using polyurethane foams of desired porous structure. Moreover, the samples can be produced in any size or shape for the desired applications. Figure 4.36 shows the HA scaffolds of different shapes and types.

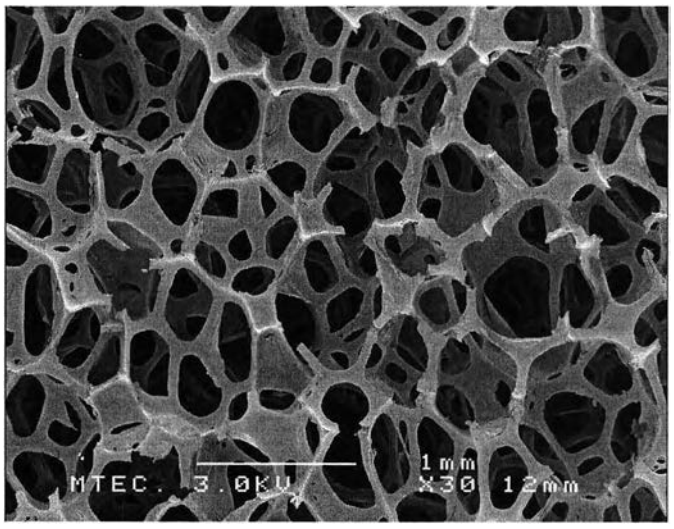

Figure 4.35 SEM micrograph showing the pores and the struts of polymer foam.

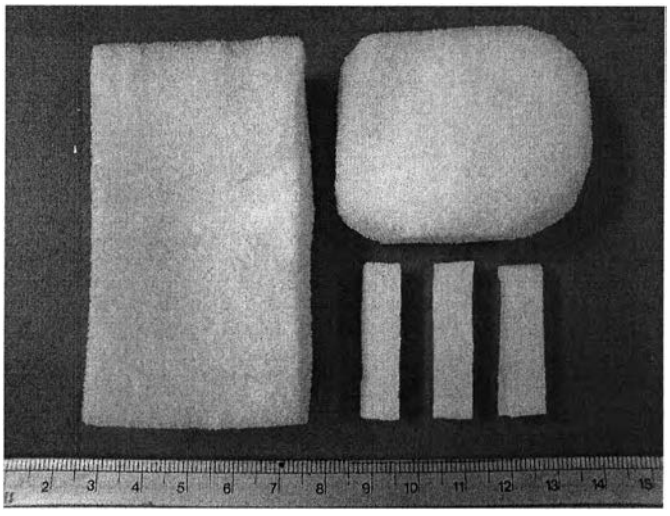

Figure 4.36 Porous HA scaffolds, made from HA with and without the additives, in different size and shape sintered at 1300 ^{o}C (The scale is centimeters.).

The surface morphologies of porous HA sintered at 1200 and 1300 °C were shown in Figure 4.37. These figure show the scaffolds have an open pore, and are highly interconnected, with a uniform porous microstructure. In the case of pure HA sintered at 1200 °C, a few cracking defects showed, with more closed pores and high porosity on the struts. Porous HA after sintering at 1300 °C for 4 h showed excellent densification. No noticeable pores and cracking on struts are observed for this sintering. The porous HA has a pore size distribution range from 100 to 420 μm at an overall porosity of 83% and wall thickness ~ 95 μm (sintering at 1300 °C). The grain size was measured to be approximately 5-10 μm. This sample exhibits a porous structure with all pores interconnected that it has some similarity to the spongeous bone. Moreover, porous HA sintered at 1300 °C was strong enough for sample handling such as cutting and grinding (Figure 4.38). Therefore, porous HA samples in this study may be used in bone tissue engineering applications and bone substitution applications. It is required that the materials possess three dimensionally interconnected pores having a pore size ~100-500 μm and high porosity (> 60% porosity). This is due to porous structure giving the advantage of allowing circulation of body fluids and increasing the potential for firm attachment of the body tissue.

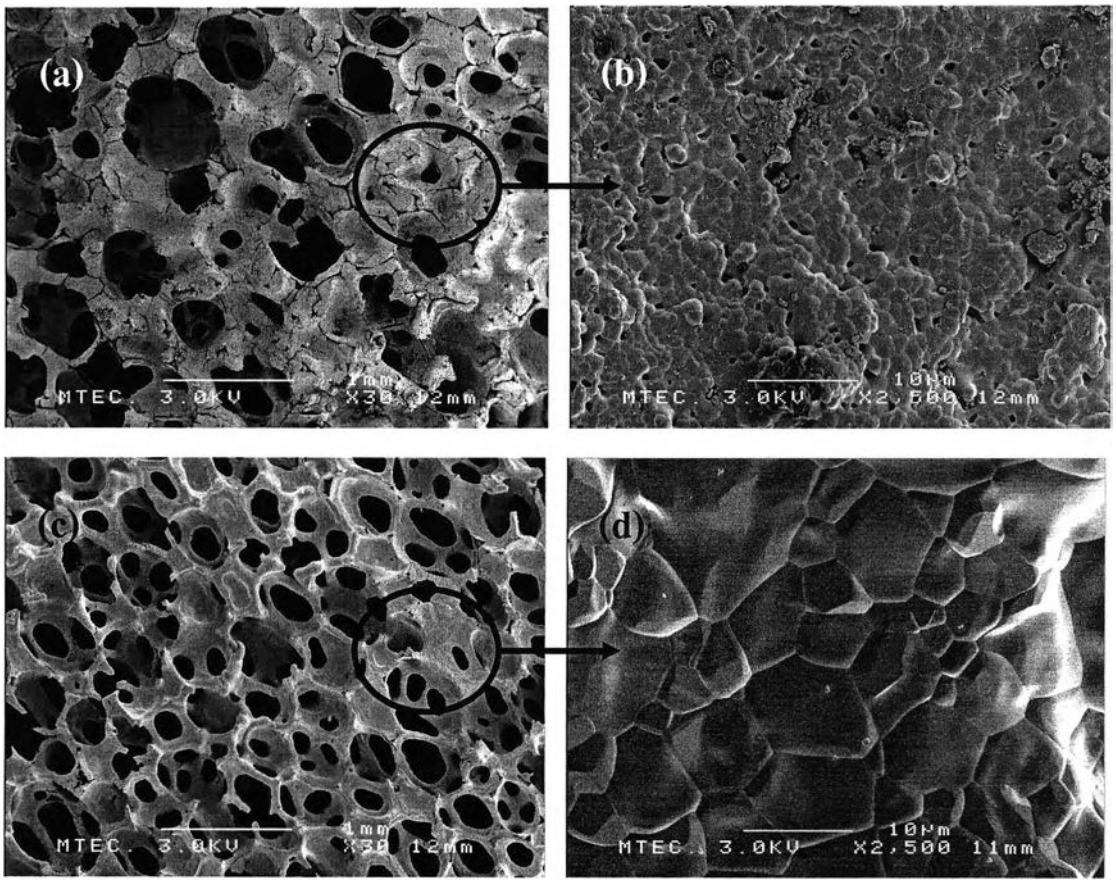

Figure 4.37 SEM micrographs of HA without glass frit additive sintered at (a-b) 1200 °C and (c-d) 1300 °C, respectively.

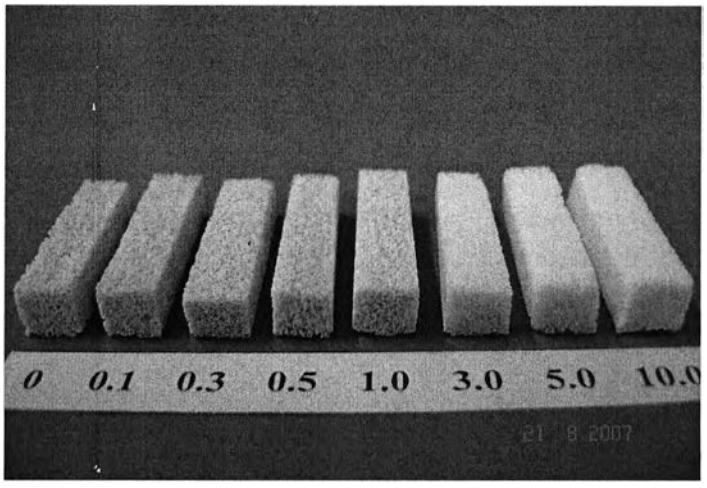

Figure 4.38 Polished surfaces of the porous HA with varied amount of glass frit additive sintered at 1300 °C.

4.4.2 Microstructural Evolution of Porous HA with Glass Frit Additives

The effects of glass additive content on porous HA morphology were considered from polymer foam fabrication, as shown in Figure 4.39. This figure shows SEM micrographs of porous HA with varied amount of glass additive, produced by the polymeric sponge method. In experimental studies, the limited glass addition 20.0wt% was observed which has not been previously reported in the literature at additive content in HA up to 10wt%. When the glass additive content increased, porosity slightly decreased. The lowest porosity was 75% for the 20wt% additive. The main reason for these trends was the increase in viscosity controlled adhesion between the slurry and polymer foam struts. The use of the glass powder remarkably, reduced the viscosity of the mixed slurry, which was believed to be highly beneficial to its preparation even with a high additive content. At low additive content, lower than 10wt%, the viscosity will be decreased with increasing additive due to the glass additive having large particle sizes. A low viscosity will favor pore coalescence and low adhesion. Moreover, the slurry tends to fast settle down (aggregate) at the bottom of the polyurethane foam during the drying process which results in a non homogeneous porous structure after sintering. Therefore, mechanical strength and density of the product do not have high values due to high porosity on the struts, and incomplete packing. On the other hand, viscosity of the slurry increased with increasing glass additive above 10.0 wt%. High viscosity will favor closed pores and high adhesion therefore decreasing porosity, but increasing pore wall thickness and mechanical strength. Additionally, high viscosity slips, with higher additive content, have resulted in foam collapse before setting of the foam structure had taken place due to the fact that the HA slip could not impregnate into the polymer foam. Figure 4.40 shows SEM micrographs of HA with 10wt% glass with different fabrication methods, sintered at 1200 $^{\circ}$C for 4 h. In the case of the polymeric sponge method, the morphology was identified as hydroxyapatite having whisker shapes. It is similar to the deposition results of HA on titanium substrate by a hydrothermal electrochemical method [62]. Meanwhile whisker shapes could not be seen after uniaxial pressing in the same composition. Figure 4.41 shows SEM micrographs of HA with 5 and 10.0 wt% SiO_2

and glass additives on wall struts sintered at 1300 °C fabricated by polymeric sponge bone process. No whisker shapes appeared in porous HA with 5.0wt% SiO_2 additive. , HA with glass formed whisker shapes in this level of glass content and increased with increasing glass content. This result supported the observation that the effect of glass additive on c-axis of caused crystal nucleation and growth of the HA. The phase structure and morphology of this whisker shapes was responsible for the improvement in physical and mechanical properties of porous HA with glass additive compared to pure HA.

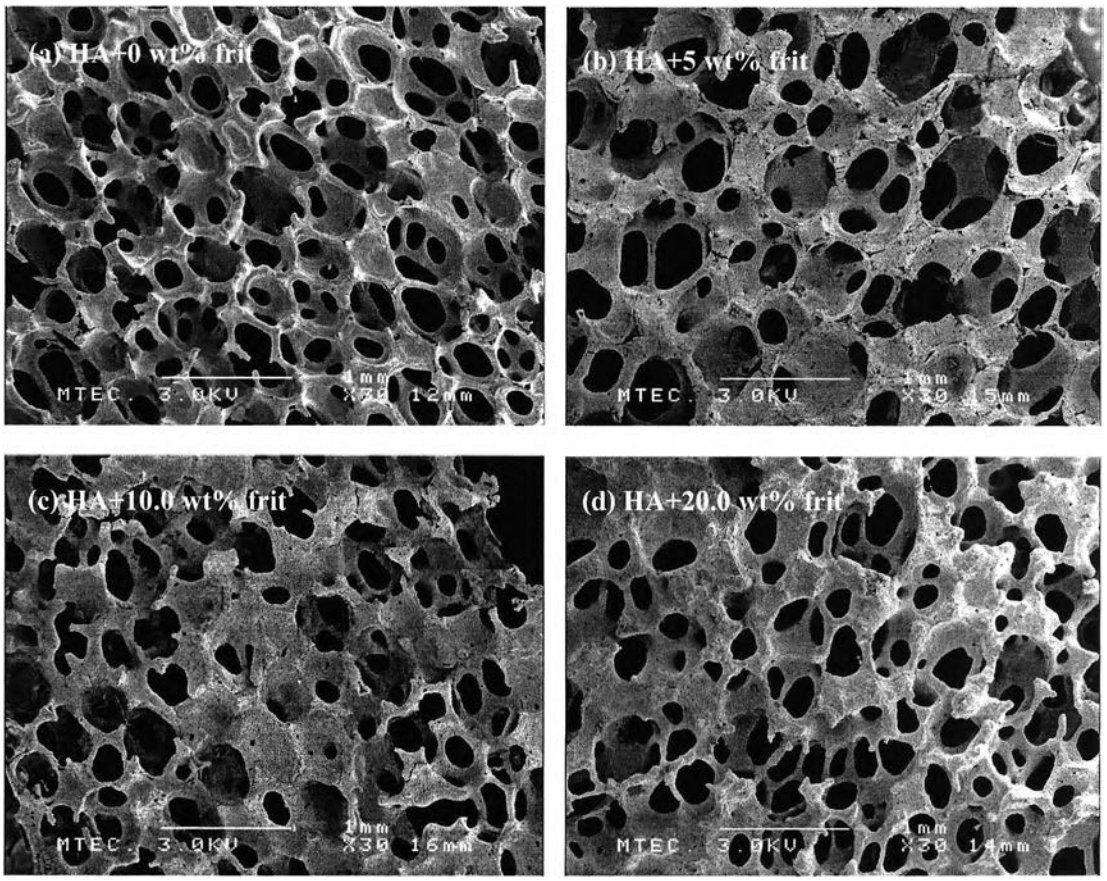

Figure 4.39 Porous HA with varied amount of glass frit additive using polymeric sponge method after sintering at 1300 °C.

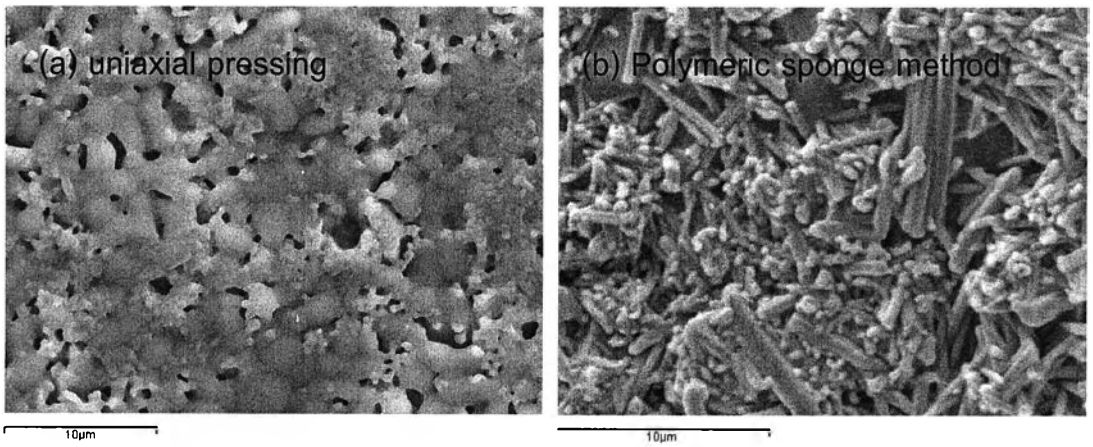

Figure 4.40 SEM micrographs of HA with 10.0 wt% glass frit additive sintered at 1200 °C and fabricated by (a) uniaxial pressing and (b) polymeric sponge method.

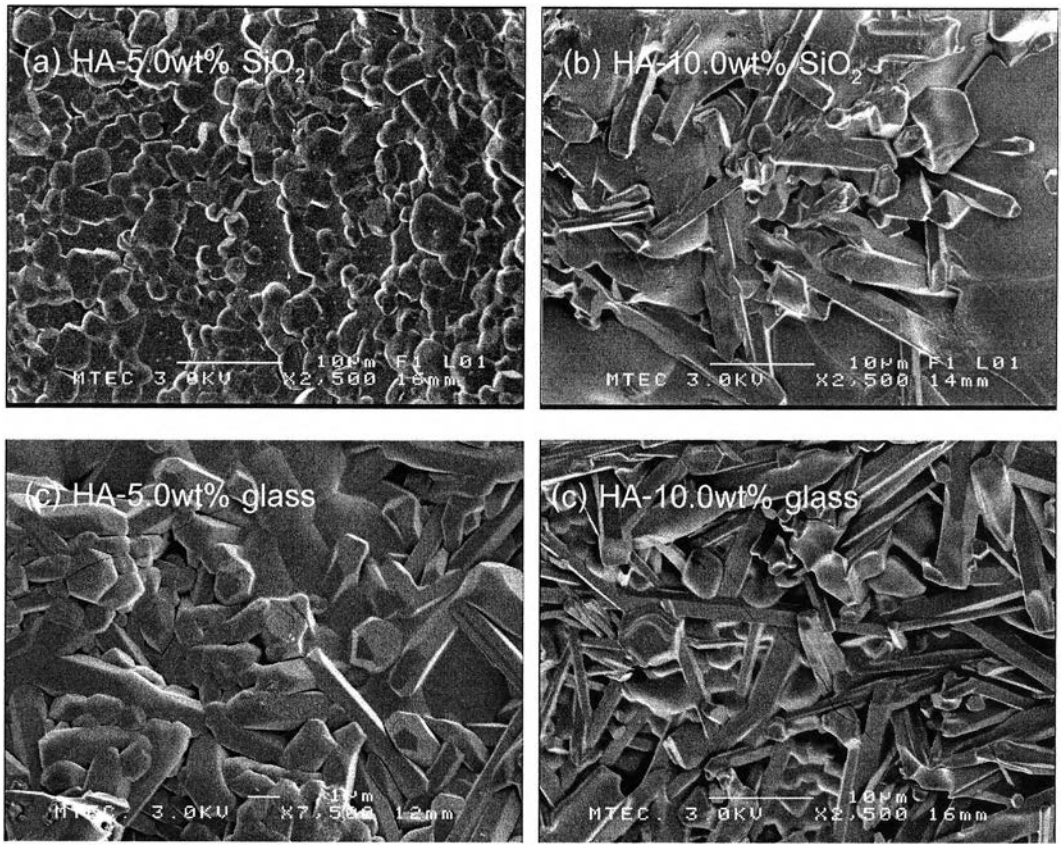

Figure 4.41 SEM micrographs of HA with 5.0wt% and 10.0wt% SiO_2 and glass frit additives sintered at 1300 °C and fabricated by polymeric sponge method.

4.4.3 Mechanical Properties of Porous HA with Glass Frit Additive

Figure 4.42 shows the effect of glass additive content on the compressive strength and porosity of the porous HA structure sintered at 1300 °C. The porous HA ceramic fabricated in this temperature is attributed to full densification compared to the other sintering. The compressive strength of HA with glass additive will be decreased with increasing amount of additive from 0.5 to 5.0 wt%. The compressive strength decreased from 1.01 to 0.67 MPa, when the additive increased from 0.5 to 3.0 wt%. After that compressive strength increased significantly with increasing additive content from 0.5 to 3.0 wt%. The highest compressive strength achieved in this study was 11 MPa for HA with 20.0wt% glass additive sintered at 1300 °C for 4 h. These values are comparable or even much higher than those reported in the literature and for sponge bone. A summary of the effect of glass and fine silica additives content and sintering temperature on the mechanical properties is shown in Appendix C. The mechanical properties of HA can be increased due to the incorporation of a glassy phase during its sintering process. A strong chemical bond is developed between HA and the glass additive at high temperature. The liquid phase acts on the solid HA particles to dissolve and reprecipitate the HA promoting the kinetics of the sintering process by a faster atomic diffusion than the concurrent solid state process pure single phase HA. As a result of this reaction TCP phases were formed and the porosity was eliminated. These reasons are all in good agreement with experimental results. The elimination of porosity in struts resulted in increased density and mechanical strength values as compared to HA sintered bodies.

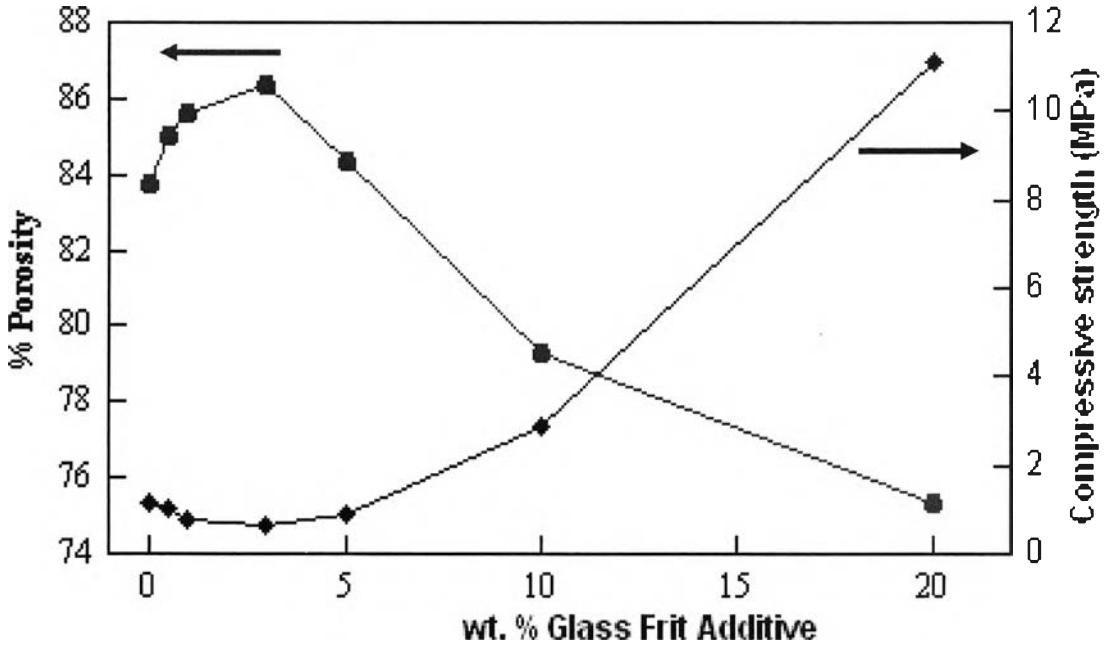

Figure 4.42 Relationship between compressive strength, porosity of HA and the varied amount of glass frit additive after sintering at 1300 °C.